Marine Geology 440 (2021) 106568

Contents lists available at ScienceDirect

Marine Geology

journal homepage: www.elsevier.com/locate/margo

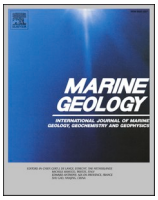

Late glacial to holocene sedimentary facies of the Eirik Drift, southern Greenland margin: Spatial and temporal variability and paleoceanographic implications

Sally Davies [a,1], Dorrik Stow [b,*], Uisdean Nicholson [b]

[a] Carrhill Road, Mossley, OL5 0BL, UK
[b] IGE-EGIS, Heriot Watt University, Edinburgh EH14 4AS, UK

ARTICLE INFO

Keywords:
Eirik Drift
Contourite sedimentation
NW Atlantic bottom currents

ABSTRACT

The Eirik Drift, off southern Greenland, is one of a series of contourite deposits in the northern North Atlantic that record changes in the strength and location of western boundary currents in the region. To date however, the sedimentary facies, and particularly the variation in facies across this drift, have received relatively little investigation. Here, we present an analysis of the sedimentary facies observed within a transect of cores from the crest to toe of the Eirik Drift from late Pleistocene to Holocene. The Holocene sequence consists of muddy contourites with high sedimentation rates at the drift toe, and a condensed sequence of sandy contourites on the upper drift flanks, consistent with winnowing under strong bottom currents on the upper drift and deposition under a low velocity, sediment-laden current at the drift toe. We interpret this to be a combined result of episodic, high-energy benthic storm events associated with the East Greenland Current (EGC) on the upper drift and more continuous, lower velocity Deep Western Boundary Current (DWBC) on the drift flanks. The deglacial interval is represented by muddy contourites across the drift, with evidence for decreasing current activity (both EGC and DWBC) and more widespread ice-rafted deposition from the Bolling-Allerod into the Younger Dryas. Palaeocurrent data from this interval show two separate current directions at the crest of the drift, suggesting temporary, local detachment of the DWBC or EGC, linked to temporal variation in current strength. The late glacial interval consists of glaciomarine hemipelagites and muddy contourites, with evidence for a higher degree of current influence at shallower depths, consistent with a moderate EGC and weak DWBC. This is the first time that the EGC is recognised as having a significant role in sedimentation on the Eirik Drift.

1. Introduction

The Atlantic Meridional Overturning (AMOC) is one of the most important components of the Earth's coupled ocean-climate system, transporting heat to high latitudes, controlling the exchange of carbon dioxide and oxygen between the oceans and atmosphere, and controlling the distribution of nutrients in the oceans (Rahmstorf, 2002, 2006). Ocean circulation, including the AMOC, is driven by a number of processes, including surface wind shear, convection, tidal mixing and the production of dense, saline water masses at high latitudes (Broecker, 1991; Dickson and Brown, 1994; Wunsch, 2002). Changes in the strength and location of Earth's currents is closely coupled to climate, with important positive and negative feedback mechanisms, to teleconnections between hemispheres, and to the location, width and sill depth of oceanic gateways (Rahmstorf, 2002).

Contourite drifts form directly under the influence of bottom currents, and their morphology and sediment facies can be used to reconstruct current dynamics (location and strength) through time (Faugères et al., 1999; Faugères and Stow, 2008). They therefore represent important repositories for the record of ocean circulation and climate change (Knutz, 2008). These drifts are typically associated with bottom currents controlled by deep thermohaline circulation, particularly western boundary currents, and build up thick accumulations of fine-grained (mud-rich) sediments (Stow and Faugères, 2008). However, the relatively low velocities typically associated with such currents are not sufficiently strong to erode, entrain and transport coarse-grained

* Corresponding author.
E-mail address: d.stow@hw.ac.uk (D. Stow).
[1] formerly at School of Ocean and Earth Science, University of Southampton, Southampton, UK

https://doi.org/10.1016/j.margeo.2021.106568
Received 8 January 2021; Received in revised form 8 July 2021; Accepted 12 July 2021
Available online 17 July 2021

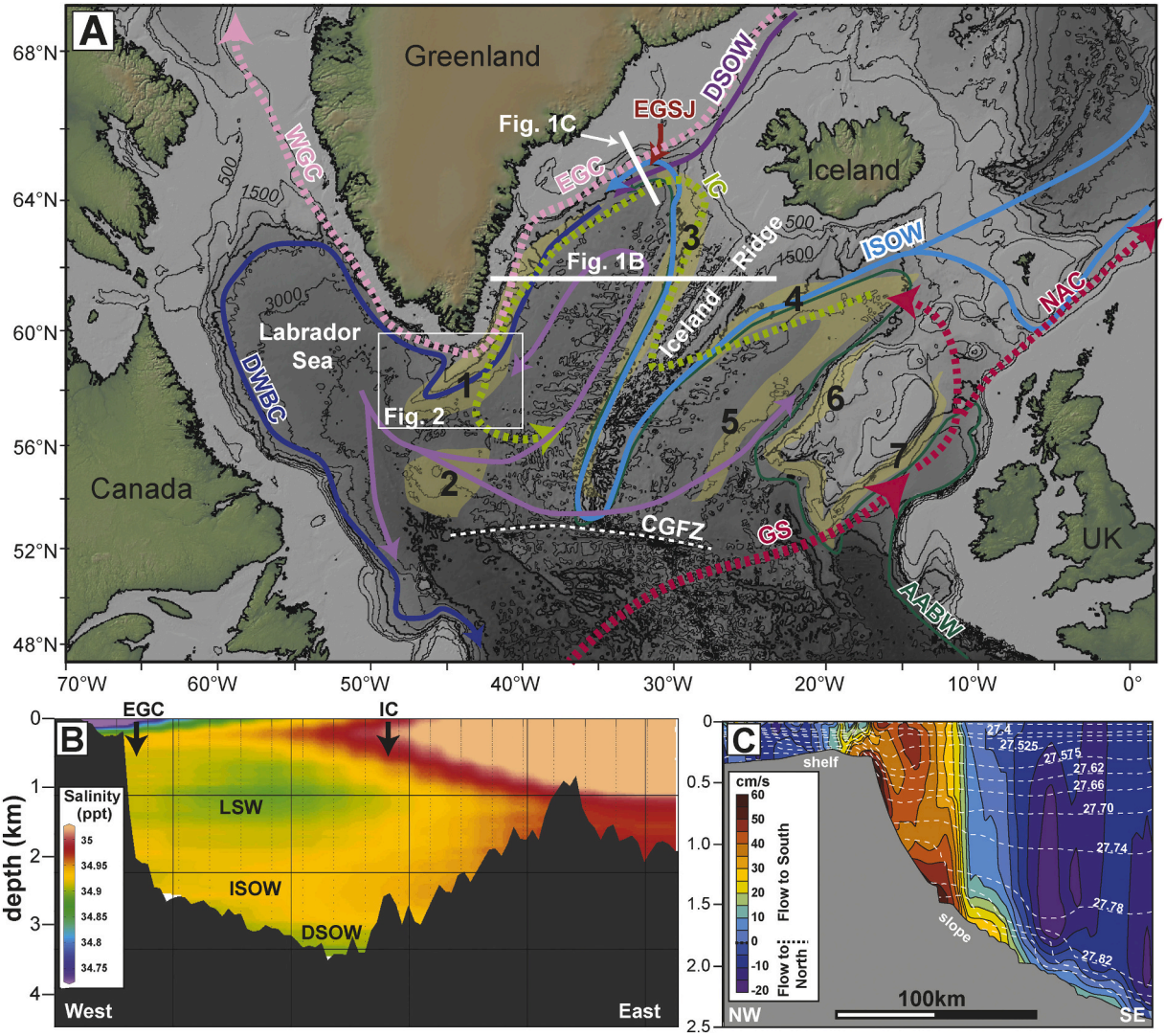

Fig. 1. (A) Location map of the Eirik Drift (Fig. 2 inset) with respect to the main surface (dashed lines) and deep (solid lines) currents in the North Atlantic. GS - Gulf Stream, NAC - North Atlantic Current, IC - Irminger Current, EGC - East Greenland Current, WGC - West Greenland Current, ISOW - Iceland Straight Overflow Water, DSOW - Denmark Strait Overflow Water, DWBC - Deep Western Boundary Current, EGSJ – East Greenland Spill Jet. Pale yellow polygons show location of North Atlantic drifts from Faugères et al. (1999), including: 1 - Eirik, 2 - Gloria, 3 - Snorri, 4 - Bjorn, 5 - Gardar, 6 - Hatton, and 7 - Feni. (B) Oceanographic cross section of the North Atlantic from the East Greenland shelf to the Iceland Ridge, showing main water masses and location of main surface currents. Salinity data is from Ocean Data View (Schlitzer, 2020) and the location of the transect shown in Fig. 1A. (C) Oceanographic cross section of the East Greenland shelf, showing absolute geostrophic velocities (colours) and potential density (kg m^{-3}) as white dashed lines. The elevated geostrophic velocities affecting the upper slope from ~400 to 1700 m are a combined result of the EGC and EGSJ. Modified from Pickart et al. (2005). (For interpretation of the references to colour in this figure legend, the reader is referred to the web version of this article.)

sediment (Bridge and Demicco, 2008).

More energetic conditions at the seafloor are commonly the result of benthic storms, the seabed expression of surface eddies and vortices. These are associated with more pervasive erosive features, and with significant winnowing of fine sediment and accumulation of coarse-grained sand sheets, which are particularly common at strong ocean fronts such as the Gulf Stream and Subantarctic Front (Gardner et al., 2017; Nicholson and Stow, 2019; Nicholson et al., 2020; Nishida et al., 2021). Cascading water masses from restricted ocean gateways and constricted flow through contourite channels can also achieve significantly higher velocities than in unconstrained western boundary currents, and are also associated with coarse-grained contourites and erosional features (Stow and Hernandez-Molina, 2013; Brackenridge et al., 2018).

The Eirik Drift lies off the southern margin of Greenland and is one of a series of large-scale contourite drifts that occur around the margins of the North Atlantic basin along the path of the Deep Western Boundary Current (DWBC) and its contributory water masses (Wold, 1994; McCave and Tucholke, 1986) (Fig. 1). The DWBC forms the western lower limb of the overturning circulation in the North Atlantic, transporting cold, dense water masses to southern latitudes, balancing the northern transfer of warm, fresh water masses by the Gulf Stream. These drifts have therefore become the focus of growing attention, due to their importance as records of DWBC variability and of wider paleoceanographic change (e.g. Hillaire-Marcel et al., 1994; Stoner et al., 1995; Bianchi and McCave, 1999; Fagel et al., 1999; Hall et al., 2004; Stanford et al., 2006). The Eirik Drift also forms beneath the East Greenland Current (EGC), a strong south-flowing surface current associated with the Polar Front, although its influence on the drift has not previously been documented (see discussion). Sedimentation in the Eirik Drift started in the Early Miocene (Müller-Michaelis et al., 2013), and the drift therefore forms an important stratigraphic repository documenting the long-term evolution of these current systems.

Here, we present new information on the late glacial to Holocene

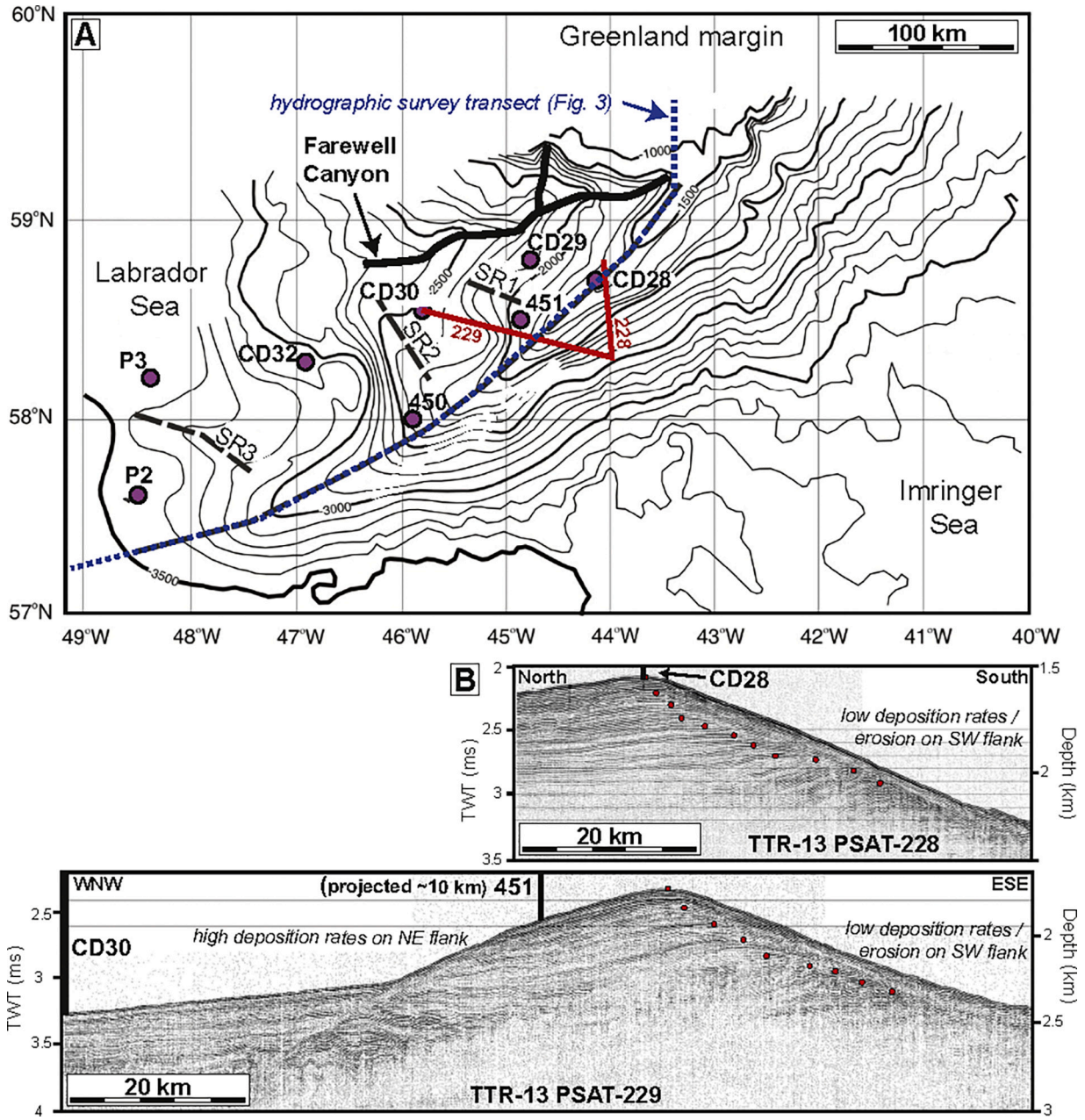

Fig. 2. (A) Detailed bathymetric map of the Eirik Drift (modified from Hunter et al., 2007a) indicating the main and secondary ridge crests, the cores used in this work (pink dots), the location of seismic refection profiles shown below (red lines), and the location of the hydrographic survey shown in Fig. 3 (blue dashed line). (B) Single channel seismic reflection profiles (from Hunter et al., 2007a) showing morphology and architecture of part of the Eirik Drift. Note reduced thickness of sediment succession on SE flank and crestal region of drift. Red circles show the progressive migration of the drift crest with time. Core locations for CD29 and 451 as shown. (For interpretation of the references to colour in this figure legend, the reader is referred to the web version of this article.)

sedimentary facies from the crest to the toe of the Eirik Drift, based on analysis of 8 sediment cores (1625 to 3492 m water depth) and the paleomagnetic orientation of sediment fabric to infer paleocurrent directions. We use these data to understand the relative role of different water masses in controlling the facies distribution in the drift and test the hypothesis that there were significant changes in the dynamics of the DWBC and EGC between the last glacial interval and the present day. We present a new understanding of the complex current control on contourite deposition, on its interaction with glaciomarine processes and on the nature of high-latitude drift systems.

2. Regional setting

2.1. Oceanographic setting

In the North Atlantic, AMOC is dominated by the Gulf Stream, which transports warm waters toward northern Europe, and the return circulation of deep and intermediate water masses, which converge to form the Deep Western Boundary Current offshore Eastern Greenland (Fig. 1) (Dickson and Brown, 1994; Rahmstorf, 2002, 2006). In addition to the Gulf Stream, there are other surface currents off Greenland associated with oceanographic fronts, including the EGC and Irminger Current (IC), which also meet and interact offshore Greenland and flow south (Fig. 1). When these water masses reach the southernmost tip of Greenland, they

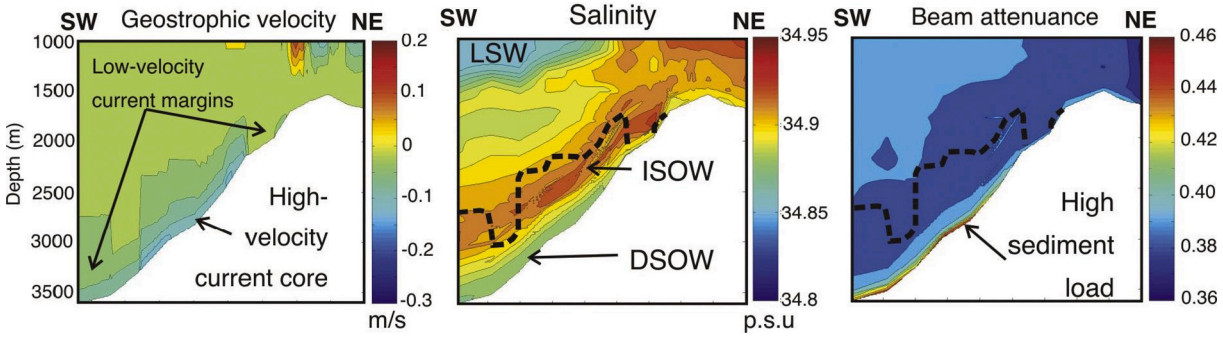

Fig. 3. Modern hydrographic data from the vicinity of the Eirik Drift (modified from Hunter et al., 2007a) showing geostrophic velocity, salinity, and beam attenuance, which can be interpreted as a proxy for sediment load. Section line runs approximately along the main drift crest (as shown on Fig. 2).

flow to the northwest, forming the West Greenland Current (WGC). The Eirik Drift forms southwards from this transition between the EGC and WGC (Fig. 2).

Hydrographic surveys in the vicinity of the Eirik Drift show that the DWBC ranges in depth from around 1800–3500 m (Fig. 3a) with a high-velocity core between 2500 and 3300 m (Hunter et al., 2007a; Bacon and Saunders, 2010; Stanford et al., 2011). The DWBC in this area is composed of four main water masses. The dominant constituents are Denmark Strait Overflow Water (DSOW) and Iceland Scotland Overflow Water (ISOW) (Dickson and Brown, 1994). These water masses cross shallow sills in the Greenland-Iceland-Scotland (GIS) ridge to the west and east of Iceland respectively and then descend rapidly, following the margins of the Irminger and Iceland basins as they flow south (Fig. 1). The DSOW has a lower temperature and salinity and higher density than ISOW, and therefore sits lower on the slope (Figs. 1b, 3b). The two overflow waters entrain a significant amount of overlying Labrador Sea Water (LSW) (Dickson and Brown, 1994; Alvarez et al., 2004) and lesser amounts of Lower Deep Water (LDW) (McCartney, 1992) along their respective routes.

The DSOW travels directly to the Eirik Drift along the east Greenland margin (Fig. 1). The ISOW, however, follows the western boundary of the Iceland Basin before passing through the Charlie Gibbs Fracture Zone then crossing the Irminger Basin via a number of different, depth-dependent paths en route to its main merging point with DSOW in the DWBC off the south east Greenland margin (Hunter et al., 2007a). At the Eirik Drift, DSOW has a relatively high sediment load compared to ISOW (Fig. 3c). This may be partly related to the difference in path length following the main points of erosion in the vicinity of GIS ridge (Hunter et al., 2007a), as well as the fact that DSOW has a higher velocity, preventing entrained sediment from settling to the seabed.

The East Greenland Current (EGC) is a surface current associated with the Polar Front, which separates cold water masses on the East Greenland Shelf from warmer and more saline water masses to the east. As it passes over the Denmark Strait, the current bifurcates, resulting in the formation of mesoscale eddies and vortices, with eddy trains extending hundreds of kilometres to the south (Almansi et al., 2020). This enhanced Eddy Kinetic Energy (EKE) results in velocities at the seafloor (often exceeding 1 m/s; Brearley et al., 2012) that are significantly higher than those in the DSOW (~10 cm/s; Lauderdale et al., 2008). Turbulence associated with these eddies also results in the entrainment of dense water masses from the East Greenland shelf, resulting in the formation of the East Greenland Spill Jet (EGSJ) (Pickart et al., 2005). These water masses cascade down the continental slope at velocities sometimes exceeding 160 cm/s (Brearley et al., 2012) until they find their equilibrium profile at around 1000 m. Recent surveys show that water masses associated with the EGSJ are equivalent (~5 Sv) to all other components of the DWBC (Brearley et al., 2012). The sedimentary response to this has not been documented.

The dynamic properties of the currents offshore Greenland have changed significantly over different timescales, from decadal-centennial (Bacon, 1997, 1998) to millennial and longer term (Holliday et al., 2007, 2009). Stable isotope data indicates that the DWBC was strong during the last interglacial, similar to the Holocene (Hillaire-Marcel et al., 1994). By contrast, during glacial stages, ocean circulation was inhibited by much more homogeneous water masses than in the Holocene (Hillaire-Marcel et al., 1994). The presence of short-lived cold periods in the North Atlantic during deglaciation – Heinrich events – are inferred to have been caused by massive freshwater input from melting glaciers, which limited or shut off the AMOC in the North Atlantic (Stanford et al., 2011). This freshwater forcing of the coupled ocean-climate system is an important component of models of future anthropogenic warming and deglaciation (e.g. Fichefet et al., 2003; Lenaerts et al., 2015). The Eirik Drift provides an important archive of these past events, including both the DWBC and EGC.

2.2. Geological setting and drift morphology

The Eirik Drift was first identified in the 1960s (Johnson and Schneider, 1969) and has been the subject of numerous investigations, including several contributions resulting from the Ocean Drilling Program Leg 105 (Srivastava et al., 1989a, 1989b). The majority of these investigations have focussed either on detailed sedimentary or isotopic characteristics at particular locations (e.g. Chough and Hesse, 1985; Aksu and Hillaire-Marcel, 1989; Aksu et al., 1989; Cremer, 1989; Hiscott et al., 1989), seismic characteristics (Hinz et al., 1979; Arthur et al., 1989; Srivastava et al., 1989a, 1989b; Hunter et al., 2007a) or paleoceanographic proxy records (Kaminski et al., 1989; Hillaire-Marcel et al., 1994; Stoner et al., 1995; Fagel et al., 2002). Differences in sedimentation rate, isotopic composition and ice-rafted debris content across the lower flanks of the drift have been discussed in relation to glacial/interglacial timescales (Hillaire-Marcel et al., 1994), in particular.

The Eirik Drift is a large, elongate, mounded deposit that extends for at least 350 km to the southwest from the steep southern Greenland slope (Fig. 2). The main crest of the drift descends from a water depth of around 1600 m adjacent to the Greenland margin to around 3500 m at the drift toe, toward the centre of the Labrador Sea. The drift has a maximum cross-sectional elevation of around 1200 m. Three secondary drift ridges trend to the northwest away from the main drift crest at approximately 90 degrees. The northern margin of the drift is delineated by a major canyon, which we refer to as the Farewell Canyon, with a lobe at its foot associated with turbidity current activity (Hunter et al., 2007b).

Seismic reflection data, including high-frequency shallow seismic (Hunter et al., 2007a, 2007b) and deep-penetration multichannel seismic data (Müller-Michaelis et al., 2013; Müller-Michaelis and Uenzelmann-Neben, 2014) have highlighted the gross morphology and internal architecture of the drift. These reveal a markedly non-depositional, winnowed to erosive crestal region and SE flank, with a semi-prolonged to prolonged high-amplitude seabed echocharacter, and

Table 1
Cores used in this study. Cores TTR13AT-450G and TTR13-AT-451G are referred to as 450 and 451 throughout the text. Similarly, cores RAPID-CD28-9P to RAPID-CD32-12P are referred to as CD28 to CD32 respectively. 1 (Kenyon et al., 2004); 2 (McCave, 2004); 3 (Bacon, 2006).

Core	Latitude (N)	Longitude (W)	Water Depth (m)	Core type	Cruise
TTR13AT-450G	57 59.99	45 49.00	2326	Gravity	TTR131
TTR13AT-451G	58 30.89	44 54.33	1927	Gravity	TTR131
RAPID-CD28-9P	58 39.03	44 12.75	1625	Piston	CD1592
RAPID-CD29-10P	58 48.00	44 51.92	2145	Piston	CD1592
RAPID-CD30-11P	58 35.93	45 45.00	2440	Piston	CD1592
RAPID-CD32-12P	58 15.00	46 59.86	3072	Piston	CD1592
D298-P2	57 35.94	48 28.84	3518	Piston	D2983
D298-P3	58 13.01	48 21.77	3492	Piston	D2982

a more depositional, aggradational toe region and NW flank with a sharp, moderate to high-amplitude seabed echo and multiple, parallel, continuous sub-bottom echoes. The toe region of the northern flank has a low to moderate amplitude seabed echo with several sub-bottom echoes, with a still expanded depositional succession. The principal depocentre of the drift has migrated steadily toward the northwest (Fig. 2; Hunter et al., 2007a).

There is still considerable uncertainty concerning the timing of opening of the major North Atlantic oceanic gateways, and hence the onset of significant water exchange and export across the Fram Strait and Greenland-Iceland-Scotland Ridge (Straume et al., 2020). Whereas there is greater consensus for the Fram Strait being partly open around 20–17 Ma and fully open from 13.7–11.2 Ma (Myhre et al., 1995a, 1995b; Jakobsson et al., 2007), there is less agreement further south. For example, estimates range from 40 to 50 Ma (Thiede and Eldholm, 1983; Hohbein et al., 2012) to 10 Ma (Denk et al., 2011) for the Faeroes-Shetland Channel, and from 35 Ma (Wold, 1994) to 6 Ma (Denk et al., 2011) for the Denmark Strait. Several authors present evidence for around 18–15 Ma for the Denmark Strait (Thiede and Eldholm, 1983; Ramsay et al., 1998; Poore et al., 2006). We might therefore expect the onset of at least a proto-DWBC from the mid-Miocene.

However, it is equally uncertain exactly when construction of the Eirik Drift began. It is possible that significant build-up only began in the Early Pliocene following the inception of significant northern-sourced bottom current activity in the Late Miocene (Arthur et al., 1989). The drift grew progressively during a Pliocene phase of active growth and southward progradation (Hunter et al., 2007b). Drift growth continued, but more slowly and in a more aggradational manner, during the Pleistocene with relatively less current influence (Arthur et al., 1989). This varied between glacial and interglacial stages. Strong bottom current flow was re-established at the onset of the Holocene (Hillaire-Marcel et al., 1994).

3. Materials and methods

3.1. Database

The main resource for this study is a sequence of 8 cores forming a depth-transect from the crest to the toe of the Eirik Drift, along its northern flank (Fig. 2). The cores comprise two gravity cores and six piston cores collected between 2004 and 2006 (Table 1). They are referred to in this paper by an abbreviated annotation – i.e. 450, 451, CD28, CD29, CD30, CD32, P2 and P3.

Table 2
Sorting classification used in this study.

Degree of sorting (phi)	Classification
1–1.6	Well sorted
1.6–2	Moderately sorted
2–2.3	Poorly sorted
2.3+	Very poorly sorted

3.2. Sedimentological analyses

The main facies present within each core have been identified based on visual logs and compositional data (smear slides), with subsequent characterisation using grain size data, geochemical and carbonate analysis. Ichnological study was carried out on all cores, and trace fossils identified from visual core inspection, digital photography and X-radiography.

Bulk sediment grain size analyses have been carried out on 112 samples, chosen to characterise the major facies present in each core. The analyses were carried out using a Malvern Mastersizer 2000 at the National Oceanography Centre, Southampton, which allows measurement of the 0.02-2000 μm fraction. Mean and modal grain sizes are reported along with the degree of sorting and the proportion of sand coarser than 150 μm, to give an estimate of the proportion of ice-rafted material present. Using the standard sorting scale (Compton, 1962), the degree of sorting for all samples analysed is poor to very poor. In order to allow better resolution and facies differentiation, we have developed a bespoke sorting classification (Table 2, Fig. 4).

3.3. Paleomagnetic analysis

Magnetic susceptibility and the anisotropy of magnetic susceptibility (AMS) have been measured on a continuous strip of 2 cm^3 samples from each core. AMS can be represented as a three-dimensional ellipsoid, with the long axis indicating the direction of greatest induced magnetisation. The degree of magnetic anisotropy (P`) largely represents the degree of grain alignment, with higher values of P` indicating a higher degree of magnetic anisotropy and therefore generally a higher degree of grain alignment. Variations in P` can therefore be interpreted in terms of changes in relative current strength (Joseph et al., 1998; Joseph et al., 2002).

The orientation of the principal axis of magnetic anisotropy in sediments and undeformed sedimentary rocks generally indicates the direction of grain alignment (Rees, 1965) and can therefore be interpreted as representing the mean flow direction. To compensate for the lack of a geographic reference direction, each core has been reoriented using the magnetic declination. The mean declination of remnant magnetism can be used as an estimate of geographic north in normal polarity, Holocene sediments (Flood et al., 1985). The data from each core has therefore been rotated to north using the average declination of remnant magnetism, measured on a representative selection of the samples, allowing the palaeocurrent direction to be estimated. The combined palaeocurrent data for the glacial to Holocene sequence in each core has then been plotted as a rose diagram.

3.4. Geochemical analysis

The composition of two cores has been analysed using an Itrax high-resolution XRF scanner at BOSCORF, Southampton. The Ca/Fe, Rb/Sr, Ti/K and Fe/K ratios are discussed. The Ca/Fe and Rb/Sr ratios reflect variations in the proportion of carbonate (biogenic and/or detrital) versus clastic material (Lackschewitz et al., 1994) and the Ti/K ratio is used to assess the relative proportions of basaltic/Mid Ocean Ridge (MOR) versus continental/cratonic-derived material present (Ballini et al., 2006). The Fe/K ratio can be used to identify redox-related diagenetic events (Croudace et al., 2006). Smear slides have been

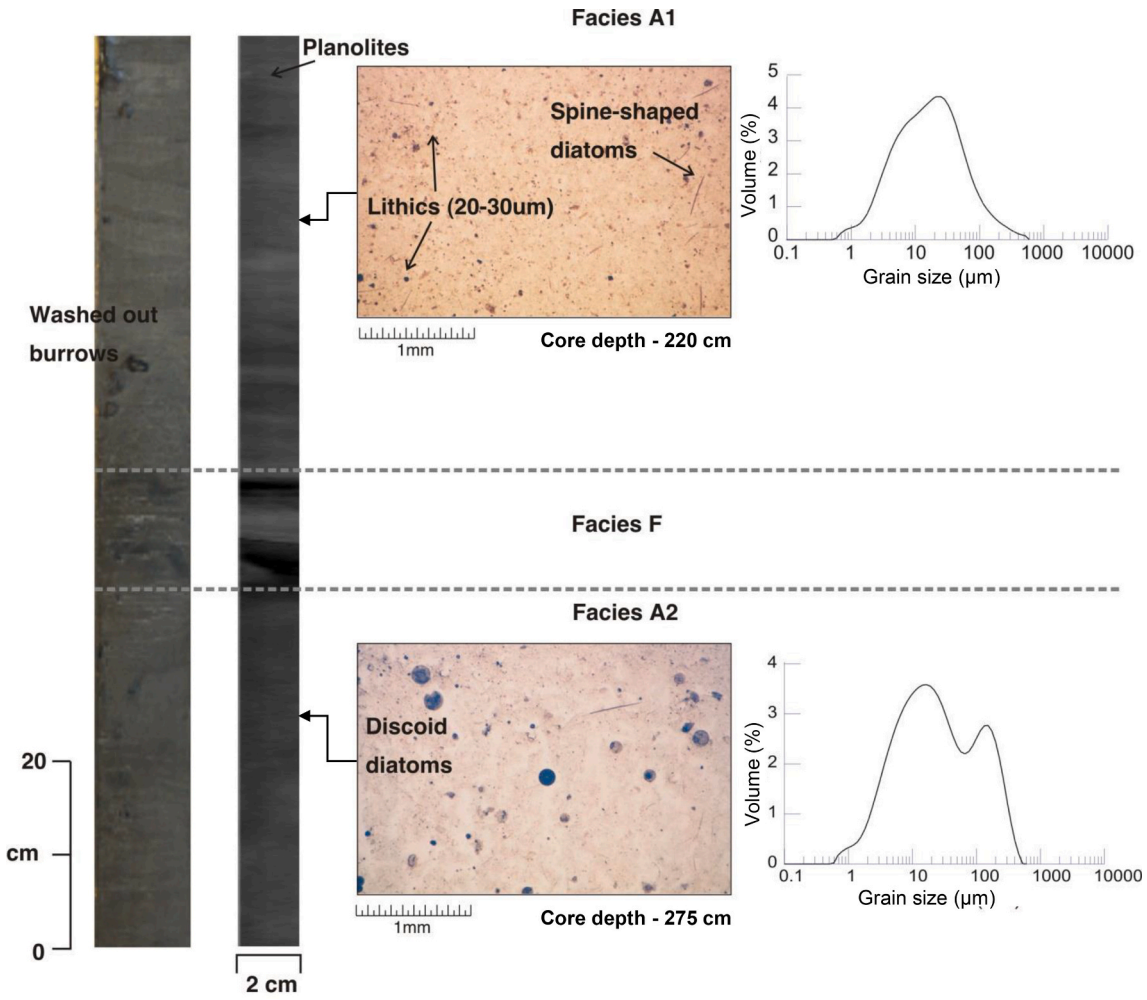

Fig. 4. Grain size distribution plots for two samples showing distinctly different grain size distributions, but a similar sorting value (poor to very poor) using the standard scale (after Compton, 1962). We have therefore modified the sorting values and terminology for use in this study so that we have a finer distinction between sorting characteristics (See Table 2). Samples used for illustration: P2-448 cm (dashed line), P3-423 cm (solid line).

made for each facies to allow further analysis of compositional variation. In addition, the carbonate content has been measured for one core using a Carlo-Erba elemental analyser.

3.5. Chronostratigraphy

For cores from the toe of the drift (P2 and P3), the age of the sequences observed has been determined based on a series of radiocarbon dates carried out on single species picks of *Neogloboquadrina pachyderma* (sinistral) and by correlation of the magnetic susceptibility records with a published, dated record from the area (Stoner et al., 1995). The radiocarbon dates acquired for this study were determined at the NERC Radiocarbon Laboratory, East Kilbride. Publication code of samples used: SUERC-11848, 13640, 13645, 13646, 13648, 13650, 13652 and 13653. Ages calibrated using Calib Version 5.01 with a 400y marine reservoir correction of zero delta R. An age model for core 451 on the upper drift flank has been determined by Stanford et al. (2006) and correlation with the other cores from the upper drift (450 and CD28 to 32) has allowed the ages of the sequences at these locations to be determined. Approximate sedimentation rates have been determined for the Holocene, deglacial and glacial sequences as far as possible.

4. Results

4.1. Sediment facies

Seven sediment facies (A-G) have been identified on the basis of sedimentary structures, grain size, ichnofacies, paleomagnetic characteristics and geochemical composition.

4.1.1. Facies A

Facies A is a homogeneous bioturbated mud. It consists of grey-brown silty clay that is thoroughly bioturbated with no clear primary sedimentary structure (Fig. 5). Greenish cm-scale bands are present throughout the unit, characterised by an irregular pellet-like texture formed from mm-scale agglomerations (micro-mudclasts) of fine material. Bioturbation comprises a combination of cm-scale *Planolites* and mm-scale *Chondrites* burrows. Some *Planolites* burrows are washed out and the inner surface lined with pellets.

The grain size ranges from 0.5-600 μm with a mean between 28 and 63 μm. Two sub-facies are distinguished, A1 and A2. Sub-facies A1 is characterised by smaller average grain sizes (< 50 μm), a unimodal grain size distribution (modes either 6–7 or 20-35 μm), and a moderate degree of sorting (1.7–2); sub-facies A2 is characterised by greater average grain sizes (> 50 μm), distinct bimodality (modes at around 20 and 100-120 μm) and poor sorting (2.07–2.15) (Table 3 and Fig. 5). No distinction between these two sub-facies can be observed by visual

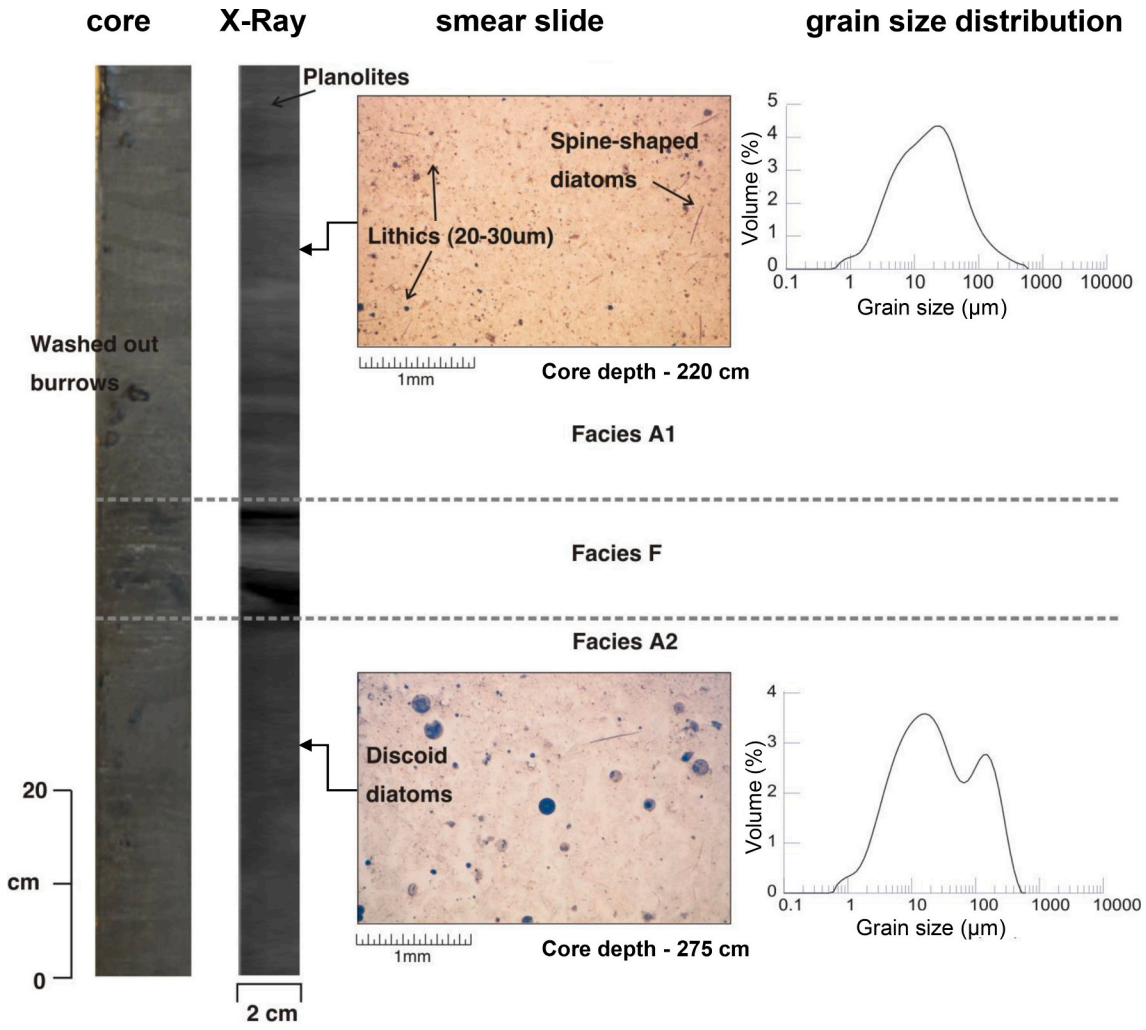

Fig. 5. Facies A - homogeneous bioturbated mud. Core photograph, x-radiograph (2 cm wide track), smear slides and grain-size distribution plots from core P3. Top section 200 cm, Base 300 cm, Facies A1 sample 220 cm, Facies A2 sample 275 cm.

Table 3
Structural and textural characteristics of the main late glacial to Holocene sedimentary facies of the Eirik Drift.

Facies	Mean (µm)	Mode 1 (µm)	Mode 2 (µm)	Sorting	% >150 µm	Primary structures	Bioturbation
A1	28–37	6–35	–	1.7–2	3–5	Green bands	Planolites Chondrites
A2	53–63	15–20	100–120	2.07–2.15	12–15	–	Planolites Chondrites
B	29–65	6–45	120	1.62–2.18	2–10	Pale bands	Planolites Chondrites Phycosiphon
C	62–124	78–103	8–10	1.91–2.24	11–22	Irregular colour banding	Planolites Chondrites
D	60–113	6–8	130–180	2.23–2.58	14–25	–	Planolites
E	132–165	118–223	~6	1.51–2.03	34–43	–	None visible
F Base	16–80	13–30	~270	1.09–1.87	1–3	Parallel lamination	None
F Upper	10–16	7–15	–	1.43–1.89	0	–	Planolites
G	79–89	6–17	~178	2.43–2.51	14–15	–	Planolites

logging of the cores, but sub-facies A2 occurs in the lower parts of the core sections and A1 in the upper parts. The degree of magnetic anisotropy within both sub-facies A1 and A2 is generally low to moderate (P` = 1.01–1.03).

The Ca/Fe ratio is low (<0.1) in sub-facies A2 and increases through sub-facies A1 to values of 0.2–0.3 in the upper 120 cm of the core sections (Fig. 6). A distinct peak, in which the ratio attains a value of 0.5–0.6, occurs in the upper few centimetres of the unit, corresponding to a light brown oxidised layer associated with the core tops. By contrast, the Rb/Sr ratio is moderate (0.15–0.3) in sub-facies A2 and decreases upward through sub-facies A1 to values of <0.1. Peaks in the Fe/K ratio correlate with the more prominent greenish bands.

This facies is composed of mixed biogenic and clastic material with a high proportion of coccoliths (Fig. 5). Comparison with the grain size data suggests that the coccoliths account for the fine mode (~6 µm) observed within sub-facies A1, while the clastic fraction accounts for the somewhat coarser mode (25-30 µm). Variability in the modal grain size in sub-facies A1 between these values is therefore interpreted to reflect variation in the proportion of clastic material versus coccoliths. Within sub-facies A2, a high proportion of both diatoms and large, platy rhyolitic volcanic glass shards were observed in the smear slides, with these constituents accounting for the sand-sized mode (100-120 µm).

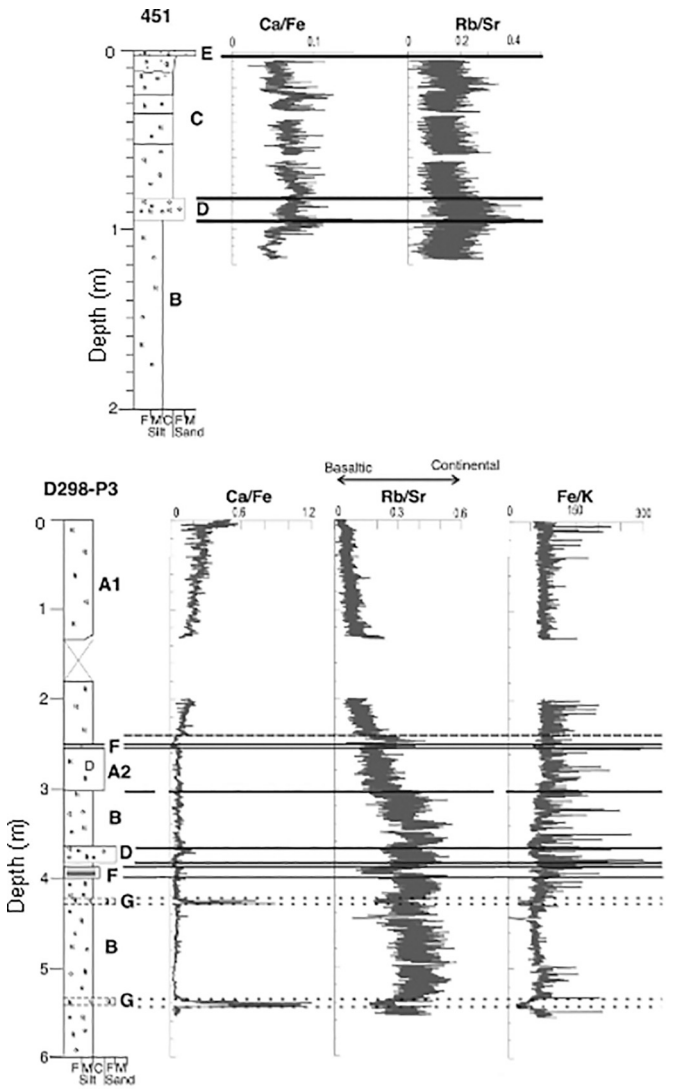

Fig. 6. Core sedimentary log, facies/sub-facies and XRF sediment composition, recording the Ca/Fe, and Rb/Sr ratios of core 451 at the main ridge and Ca/Fe, Rb/Sr, and Rb/Sr ratios of core P3 at the toe of Eirik drift. Facies as indicated against core logs on left. Vertical scale in metres.

4.1.2. Facies B

Facies B is a brown to grey-brown homogeneous bioturbated sandy mud with no primary sedimentary structure and scattered sand to cobble-sized ice-rafted debris (IRD, less than 10% >150 μm fraction). Pale coloured, fine-grained bands are present in cores CD30 and CD32. Bioturbation comprises dispersed mottling as well as distinct *Planolites* and *Chondrites* burrows throughout, while in cores P2 and P3, intervals of *Phycosiphon* are present at 540–595 cm and 300–360 cm respectively.

The bulk grain size ranges between 0.4 and 1100 μm, although a few grains greater than 2 mm in diameter were removed by sieving prior to grain size analysis, including a mafic igneous cobble 9 cm in diameter from the base of core P3. The mean grain size ranges between 29 and 65 μm and the dominant mode between 6 and 45 μm (Table 3 and Fig. 7). Secondary modes at around 120 μm are present in some deep-water cores (P2, CD30). The degree of sorting is moderate to poor (1.62–2.18) and the degree of grain alignment is generally low ($P' = 1.01–1.02$).

This facies has a low (<0.1) Ca/Fe ratio (Fig. 6), a low proportion of coccoliths and foraminifera, and a moderate to high (0.2–0.5) Rb/Sr ratio (Fig. 6).

4.1.3. Facies C

Facies C is brown homogeneous bioturbated sandy mud and muddy sand with limited primary sedimentary structure and abundant sand to pebble sized IRD (11–22% >150 μm fraction). Irregular, roughly parallel bands of darker, rust-brown colour are visible in most sections. The sediment is thoroughly bioturbated with *Planolites* and *Chondrites* burrows present throughout.

The grain size ranges between 0.5 and 1100 μm with a mean of 62–124 μm and a mode of 78–103 μm (Table 3 and Fig. 7). Secondary modes at 8–10 μm are present within some samples and the degree of sorting is generally poor throughout (1.91–2.24). The degree of grain alignment ranges from low to high ($P' = 1.01–1.05$). The Ca/Fe ratio is moderate (0.06–0.1) and the Rb/Sr ratio low (~0.15) (Fig. 6). Smear slide analysis shows the coarse fraction to be dominantly composed of lithic material (Fig. 7).

4.1.4. Facies D

Facies D is a brown homogeneous bioturbated sandy mud and muddy sand with no primary sedimentary structure and a particularly high proportion of coarse IRD (14–25% >150 μm fraction, Fig. 7). This facies occurs as very thin to medium thick units (2–20 cm) intercalated with other facies. There is no primary sedimentary structure and only indistinct bioturbation, except at the upper and lower contacts where it is more pronounced. The mean grain size ranges from 60 to 113 μm and is characterised by strong bimodality (modes at 6–8 and 130–180 μm), and with very poor sorting (2.23–2.58). The degree of grain alignment is generally very low ($P` \sim 1.005$).

There is a low Ca/Fe ratio and high Rb/Sr (Fig. 6), and a very limited biogenic component. Most of the fraction in excess of 100 μm is composed of lithic grains and (Fig. 7).

4.1.5. Facies E

Facies E is a homogeneous muddy sand. It occurs as thin (1–5 cm), poorly consolidated sandy layers that are thoroughly homogeneous with no primary sedimentary structure and no visible bioturbation. The facies is composed of 65–90% sand with a grain size range of 0.7–1100 μm. The sediments are moderately to well sorted (1.51–2.03) with a mean grain size of 132–165 μm and a well-defined mode of 118–233 μm. A minor clay-silt tail can be observed in the grain size distribution, with less common secondary mode at ~6 μm (Fig. 8). Values of P' are generally high ($P' < 1.06$).

XRF data are not available for this facies due to the poorly consolidated nature of the sediments. Smear slides show the sand-sized fraction to be composed of clastic material (largely quartz and feldspar) and dark-stained foraminifera. Abundant coccoliths are present in the fine fraction (Fig. 8).

4.1.6. Facies F

Facies F is composed of normally graded mud with a silt-laminated basal division. It occurs in distinct beds up to 60 cm thick, with a black, laminated silt base grading up into homogeneous, bioturbated fine-grained brown silty mud. Bioturbation occurs near the tops of beds, with *Planolites* burrows that are often washed out (Fig. 9). The upper boundary of these beds grades in to the overlying facies. Within the basal division the grain size ranges from 0.6 to 300 μm with a mean of 16–80 μm and mode of 15–30 μm, with a high degree of sorting (1.09–1.87). The homogeneous upper portion shows a grain size ranging from 0.4 to 250 μm with a mean of 10–16 μm and a mode of 7–15 μm and a somewhat lower degree of sorting (1.43–1.89).

Facies F has a low Ca/Fe ratio and a moderately high Rb/Sr ratio. There is a very low biogenic content, except for a foraminiferal sand layer at the base of one bed that shows as a distinct secondary mode in the grain size distribution at around 270 μm.

4.1.7. Facies G

Facies G comprises pale coloured carbonate-rich muddy sand or

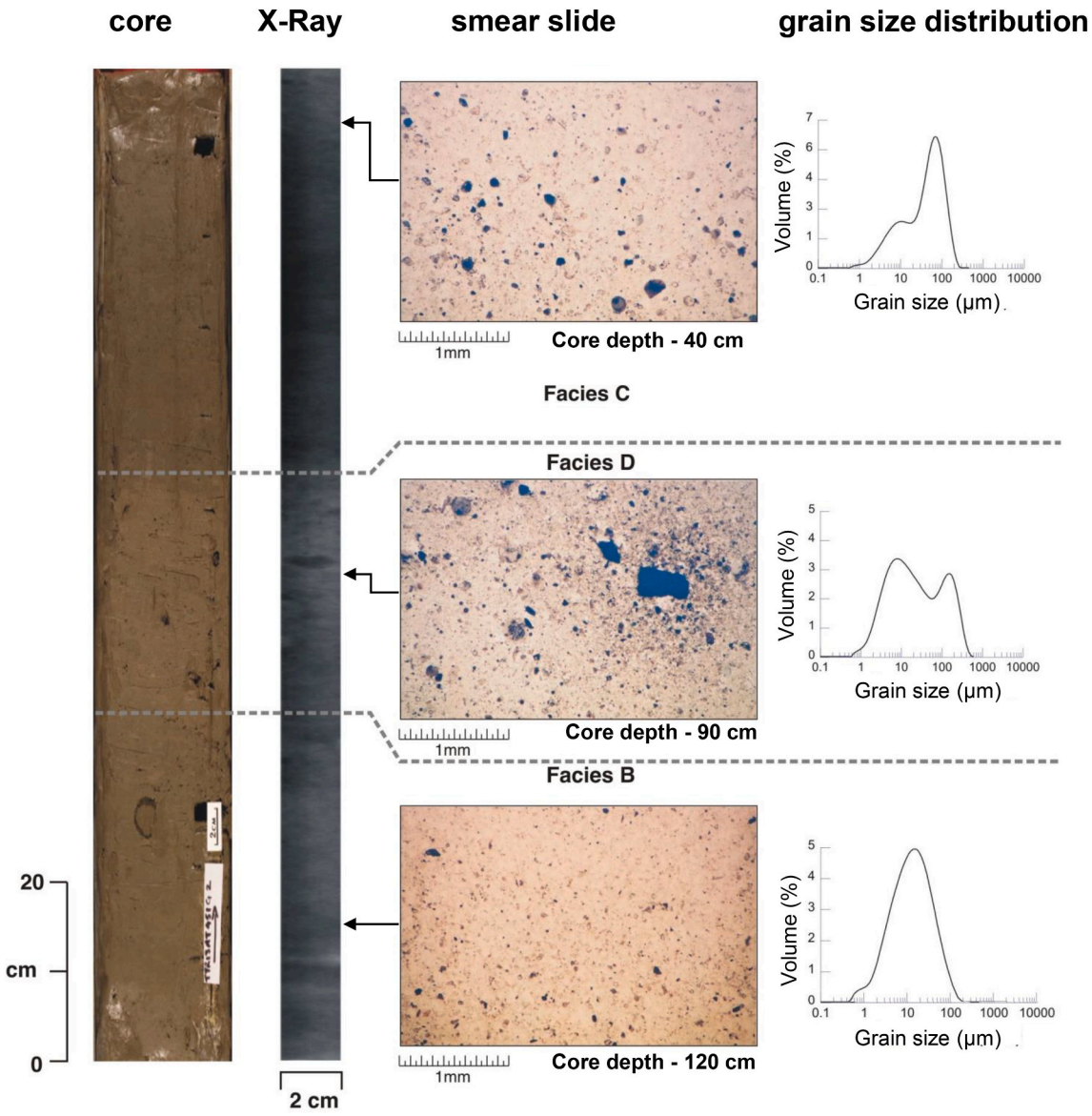

Fig. 7. Facies B - homogeneous bioturbated sandy mud with scattered IRD, Facies C - homogeneous bioturbated sandy mud with abundant IRD, and Facies D - homogeneous bioturbated sandy mud with abundant IRD and bimodal grain size. Core photograph, x-radiograph (2 cm wide track), smear slides and grain-size distribution plots from core 451. Top section 35 cm, Base 135 cm, Facies C sample 40 cm, Facies D sample 90 cm, Facies B sample 120 cm.

sandy mud. This occurs in beds up to 6 cm thick that are strongly bioturbated and show no primary sedimentary structure. The facies is very poorly sorted (2.43–2.51) with a mean grain size of 80–88 μm and a primary mode of 6–17 μm (Fig. 9). The grain size distribution is generally bimodal with a second mode at around 178 μm. These layers also show a high degree of grain alignment (P′ - 1.02-107).

The facies is characterised by a very high Ca/Fe ratio and a low Rb/Sr ratio. There is a very high proportion of fine detrital carbonate material (Fig. 9), and a sand-sized fraction (around 28%) composed primarily of clastic material (largely quartz).

4.2. Chronostratigraphy and sedimentation rates

A general chronostratigraphic framework has been developed for the transect of cores based on 8 new radiocarbon dates from cores P2, P3 and 450, a further 5 published radiocarbon dates (Stanford et al., 2006), and correlation of magnetic susceptibility records for all cores. These data and correlation are shown in Fig. 10. Three main time intervals are dated: the Holocene, deglacial (including Bolling-Allerod and Younger Dryas) and late glacial (Fig. 11).

Sedimentation rates for each of these intervals can be estimated for different parts of the drift, based on our own chronostratigraphy and on earlier data presented by Hillaire-Marcel et al. (1994) (Table 4). The sedimentation rate for the Holocene ranges from around 32 cm/ka at the drift toe to 2.3 cm/ka on the lower drift flanks (2800 m) and to 0.25 cm/ka on the upper drift flanks and drift crest.

Due to lack of precise stratigraphic resolution within the deglacial sequence, we have determined sedimentation rates for the deglacial period as a whole. The deglacial sequence shows moderate to high sedimentation rates across the drift, reaching a maximum of ~26 cm/ka in core 451 on the upper drift flank (Table 4).

The late glacial sequence shows significant difference in sedimentation rate with depth and location on the drift (Table 4). Hillaire-Marcel et al. (1994) report a moderate sedimentation rate for the deep-water drift toe (10-15 cm/ka at 3380 m) and lower drift flanks (~15 cm/ka at 2805 m), while radiocarbon dating from core 450 (this study) suggests sedimentation rates increase to around 28 cm/ka on the upper drift flanks (2326 m).

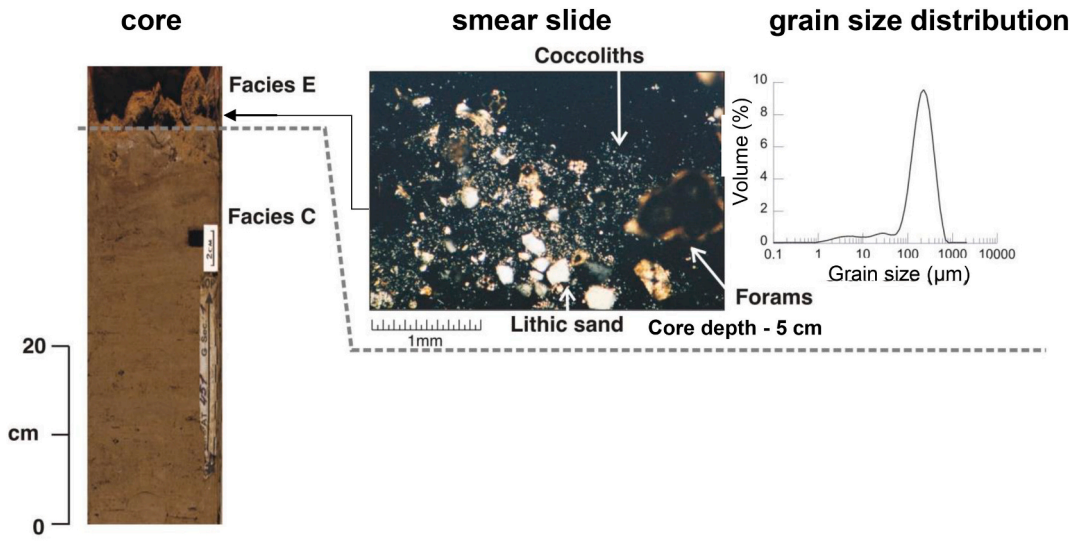

Fig. 8. Facies E - homogeneous muddy sand. Core photograph, x-radiograph (2 cm wide track), smear slides and grain-size distribution plots from core 451. Top section 0 cm, Base 48 cm, Facies E sample 5 cm.

4.3. Paleocurrent data

Paleomagnetic palaeocurrent data for the combined late glacial to Holocene sequences in all cores are plotted in Fig. 12. These generally indicate bottom current flow parallel to the local bathymetric contours, but with some notable variation. The method gives a flow orientation that is bidirectional – for example, the flow could be either to the east or west. We have therefore used a knowledge of the dominant flow direction of the modern DWBC, from hydrographic data, to interpret which direction is most likely. The observed dominance of contour-following palaeocurrents is significant, but number of local anomalies can also be observed: (a) data from core CD28, at 1625 m water depth, indicate flow northward over the drift crest; (b) data from core CD29 on the northern drift flank, indicate flow to the southeast (or northwest), rather than along contours; and (c) two dominant current directions are observed in core 450, close to the ridge crest, at approximately 45 degrees to each other. (See Fig. 13.)

Palaeocurrent directions have been plotted separately for Facies F in cores P2 and P3 (in green on Fig. 12). This facies is interpreted below as turbidites. The flow direction is approximately north-south in core P2, which is more or less parallel to the slope contours, and more variable in P3, with flow in both NE-SW and NW-SE directions indicated, approximately parallel and perpendicular to the local slope direction, respectively.

5. Interpretation and discussion

5.1. Facies and process interpretation

The regional context provides the first step toward facies interpretation. The Eirik Drift is an elongate mounded contourite drift (sensu Faugères et al., 1999; Stow et al., 2002), which has been built upwards and outwards from the Cape Farewell continental margin of southern Greenland (Johnson and Schneider, 1969; Hunter et al., 2007a, 2007b). It is an example of a high latitude contourite drift, which is likely to be influenced by glaciomarine processes. At the present day, it is swept by a system of surface and deepwater bottom currents, and these are assumed to have been responsible for its growth and development, at least since the early Pliocene (Arthur et al., 1989; Hunter et al., 2007a; Bacon and Saunders, 2010; Stanford et al., 2011).

Within this context, and by comparison with standard deepwater facies models as synthesised by Stow and Piper (1984) and Stow and Smillie (2020), our detailed observations of facies characteristics for the Eirik Drift sediments allow us to make the following interpretations.

Facies A is interpreted as a muddy contourite deposit with a moderate to high biogenic input. The degree of magnetic anisotropy within both sub-facies A1 and A2 is generally low to moderate (P` = 1.01–1.03). This, combined with the fine modal grain size suggests low current velocities. There is a greater glaciomarine signature indicated by IRD in sub-facies A2.

Facies B is interpreted as hemipelagic to low energy contourite deposition in a glaciomarine setting. Generally low current velocities are indicated by both the low P` and low dominant modal grain size, while the presence of clastic material >150 μm is indicative of ice-rafted deposition.

Facies C is interpreted to reflect contourite deposition in a glaciomarine setting, with a somewhat higher proportion of IRD than Facies B. The larger mean grain size and generally higher P` indicate a more pronounced current influence on deposition.

Facies D is interpreted as a glaciomarine hemipelagite, with a high proportion of IRD, and little to no current influence as indicated by the very poor sorting and low P`.

Facies E is interpreted as a sandy contourite formed in a glaciomarine setting. The low proportion of fine material and high degree of grain alignment indicate strong bottom current activity.

Facies F is interpreted to be the result of turbidity current deposition. These turbidites only occur at the deep-water toe of the drift, five in core P2 and two in core P3. The turbidites are thicker and more complete in P2, probably due to the partial bypass of the P3 site.

Facies G represents detrital carbonate layers, which have been described in the Labrador Basin by several previous authors (Andrews and Tedesco, 1992; Hillaire-Marcel et al., 1994; Hesse and Khodabakhsh, 1998) and have been interpreted as reflecting a combination of turbidity flow, debris flow and ice-rafting processes.

In summary, the facies observed in this study in the transect of cores from drift crest to toe are dominated by contourites and hemipelagites, with some interbedded turbidites in the toe region. The contourites are mostly muddy, with intense bioturbation throughout, a marked lack of primary sedimentary structures, moderate to poor sorting, and a mixed terrigenous-biogenic composition. Thin sandy contourites are locally present in the crestal region, and display a lack of clear bioturbation or primary structures, moderate to good sorting, and a similar mixed composition. There is very little to distinguish the muddy contourites from hemipelagic facies. Marginally greater current influence during

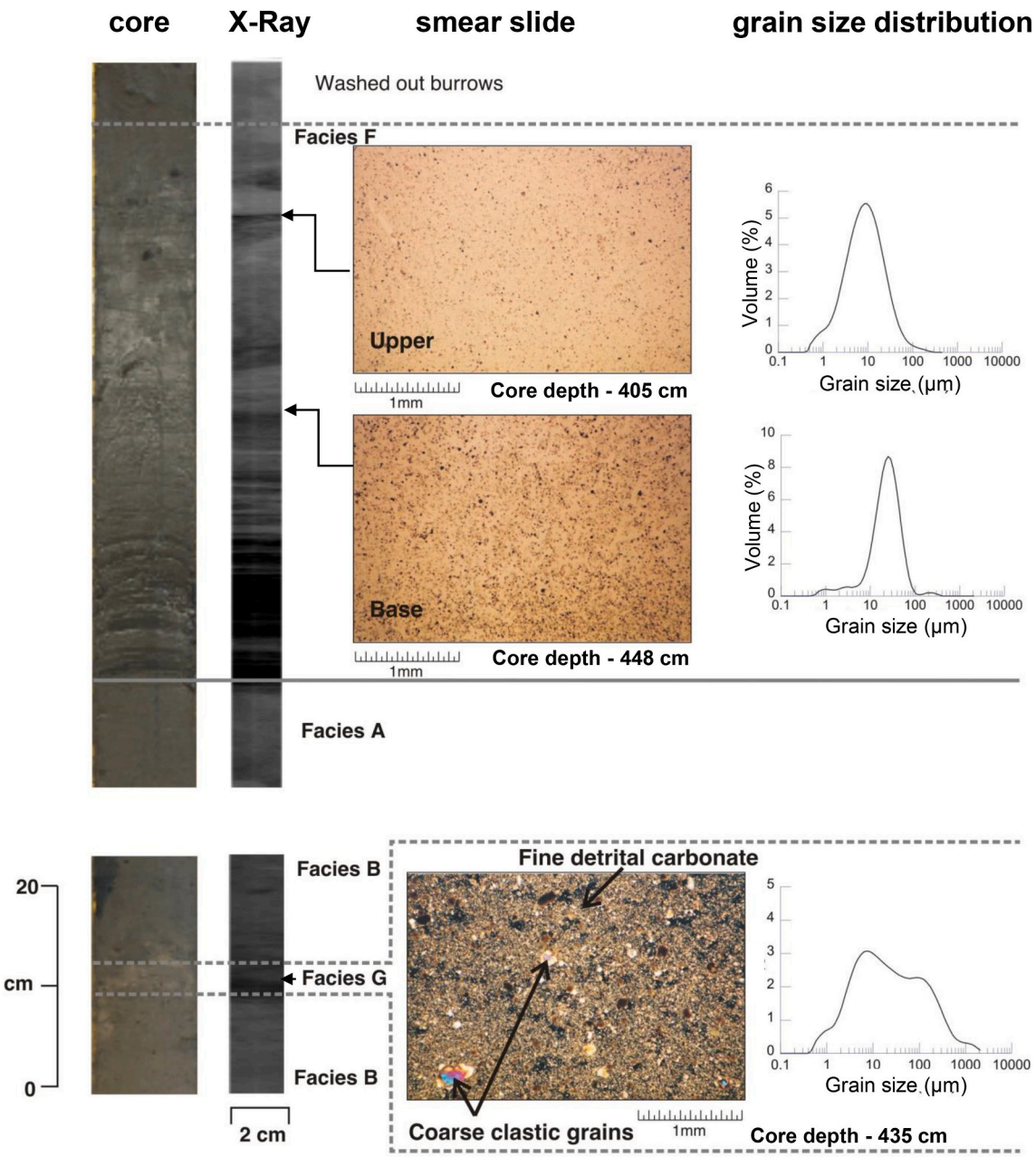

Fig. 9. Facies F - graded, silt-laminated mud, and Facies G - carbonate-rich sandy mud. Core photograph, x-radiograph (2 cm wide track), smear slides and grain-size distribution plots from cores P2 and P3. Core P2, top section (upper) 390 cm, Base 460 cm, Facies F(upper) sample 405 cm, Facies F(base) sample 448 cm. Core P3, top section (lower) 412 cm, Base 435 cm, Facies G sample 423 cm.

contourite deposition is evidenced by a slightly higher degree of magnetic anisotropy, an elevated modal grain size and better sorting (McCave et al., 2006; Stow and Smillie, 2020). Clearly, a large amount of vertical (hemipelagic) settling as well as lateral advection contributes to muddy contourite deposition.

The standard vertical sequence of facies (C1 to C5) as defined in the contourite facies model (Gonthier et al., 1984; Stow et al., 2002; Stow and Smillie, 2020) is poorly developed in the toe region and only present as a partial, base-only sequence (C1-C2-C3) in the upper 1–2 m of the crestal region. This is indicated by an upward coarsening change from Facies B to C to E, which is taken to represent an upward increase in bottom current velocity over the drift crest from Younger Dryas to the present day. Other subtle variations in grain size are noted through parts of the cores that can be related to compositional changes. These have been caused by variation in pelagic biogenic input, variation in the influx of glaciomarine IRD material, and episodic input from turbidity currents in the toe region, and are not, therefore, solely indicative of temporal changes in mean bottom current velocity. These data clearly demonstrate the need for a careful multi-proxy approach in the paleoceanographic interpretation of contourite successions.

5.2. *Provenance*

As with other drift systems (Stow et al., 2008; Bankole et al., 2020), sediment is supplied to the Eirik Drift via a combination of vertical settling of pelagic-hemipelagic-glaciomarine material, alongslope transport in bottom currents reflecting an upstream source, and direct lateral input from turbidity currents and spillover processes from the adjacent shelf/slope. Petrographic and geochemical characteristics show some variations for the different facies. We use the Ca/Fe ratio to

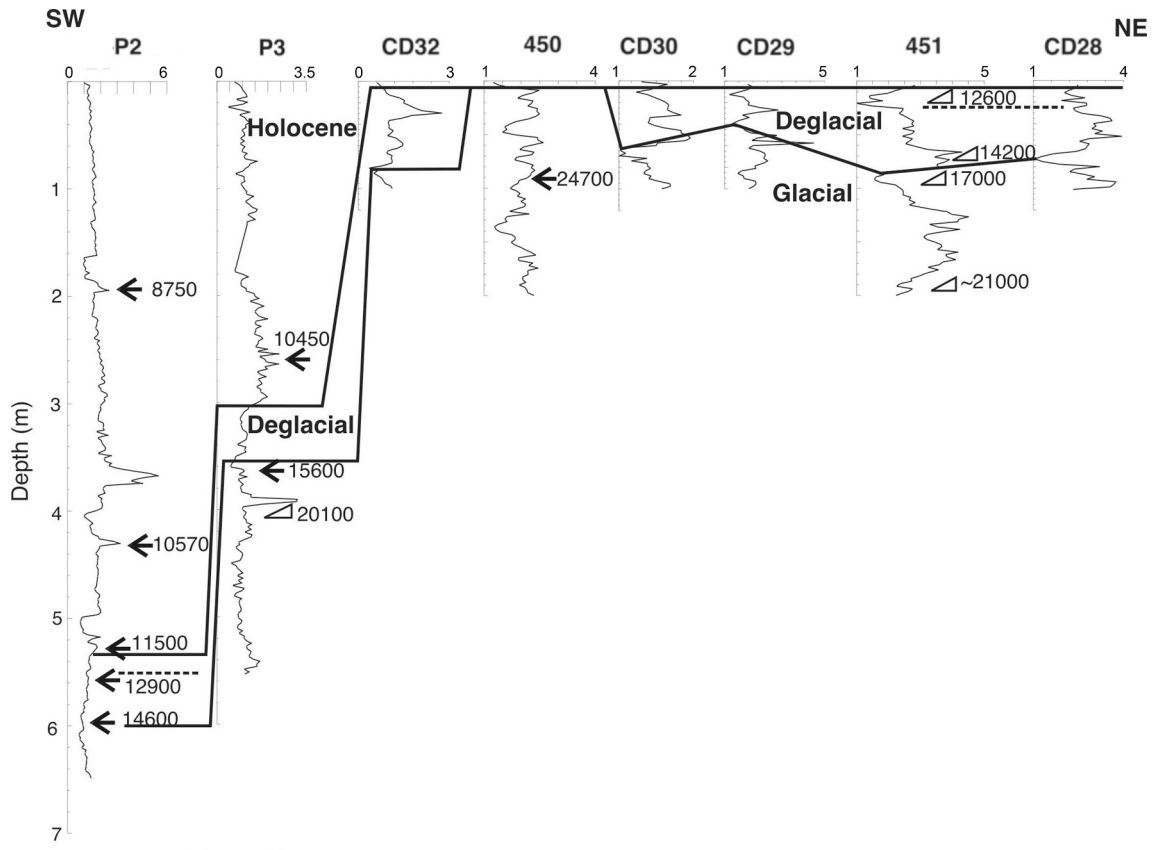

Fig. 10. Age determination and core correlation based on C14 dating and magnetic susceptibility records. The arrows show radiocarbon ages acquired as part of this study. The triangles show published radiocarbon ages.

infer increased calcareous biogenic (higher ratio) versus clastic (lower ratio) components. Similarly, the Rb/Sr ratio is taken to reflect an increasing proportion of continental/cratonic (higher ratio) versus basaltic (lower ratio) material.

The dominantly basaltic origin of the clastic fraction in Facies A (inferred from the Rb/Sr ratio) is consistent with the majority of the Holocene sediment deposited at the Eirik Drift having been eroded from the Nordic Basaltic Province in the vicinity of the Denmark Strait, and then transported a distance of ~1500 km to the drift in the DSOW portion of the DWBC (Innocent et al., 1997; Hunter et al., 2007a).

The main difference between the two sub-facies is compositional, with A2 having a high component of diatoms and volcanic glass, lower biogenic carbonate and a somewhat higher basaltic influence. The transition between these two sub-facies is gradational, showing an upward increase in calcareous biogenic versus clastic component, and in basaltic versus continental/cratonic provenance. The abundant rhyolitic glass shards are thought to have been transported to the Eirik Drift by bottom currents from closer to Iceland (the main source of volcanic glass in the region). This also represents a transport distance of around 1200–1500 km from source.

Facies E, found at the present-day sediment surface, appears to be a current-winnowed residue of both continent-derived clastic and pelagic-benthic biogenic material, typical of mixed provenance sandy contourites (Stow et al., 2008; Bankole et al., 2020).

The de-glacial and glacial facies formed under relatively weak bottom currents (Facies B and C) or from mainly hemipelagic processes (Facies D) show rather less biogenic input compared with the Holocene, and a lesser basaltic signature. The provenance signature varies, but the relatively high influence of continental/cratonic material is consistent with the ice-rafted component having been transported to the area by the East Greenland Current (EGC). Ice carried by the modern EGC derives from the Arctic Ocean and East Greenland glaciers (e.g. Andrews et al., 1997) and provenance studies have shown that dropstones deposited by the EGC comprise around 46% continental material (largely felsic/intermediate plutonics and orthogneiss) (Linthout et al., 2000).

Both Facies F and G are inferred to result, at least in part, from downslope processes. For Facies F, the dominant continental/cratonic provenance is consistent with the interpretation that the turbidites in this area derive from south-western Greenland via the Farewell Canyon, to the north of the Eirik Drift (Hunter et al., 2007b). Whereas, for Facies G, the transport of detrital carbonate material into the Labrador Basin is believed to have been from the Canadian Laurentide margin at times when ice streams extended to the shelf break (Andrews and Tedesco, 1992; Stoner et al., 1996).

5.3. *Spatial and temporal variability*

An analysis of the spatial and temporal variability in characteristics of the Holocene, deglacial and glacial facies has allowed paleoceanographic conditions under which these facies were deposited to be examined in further detail.

5.3.1. *Holocene sequence*

Holocene sediments consist of winnowed sands across the majority of the drift and thick muddy contourites at the drift toe. This difference is consistent with the observations made from previous studies (Hunter et al., 2007a, 2007b; Hillaire-Marcel et al., 1994) of sediment winnowing under strong currents across the majority of the drift, with active Holocene sedimentation limited to the drift toe, and relates to spatial variation in velocity and sediment load within the DWBC.

The sandy lag sediments on the upper drift show a maximum

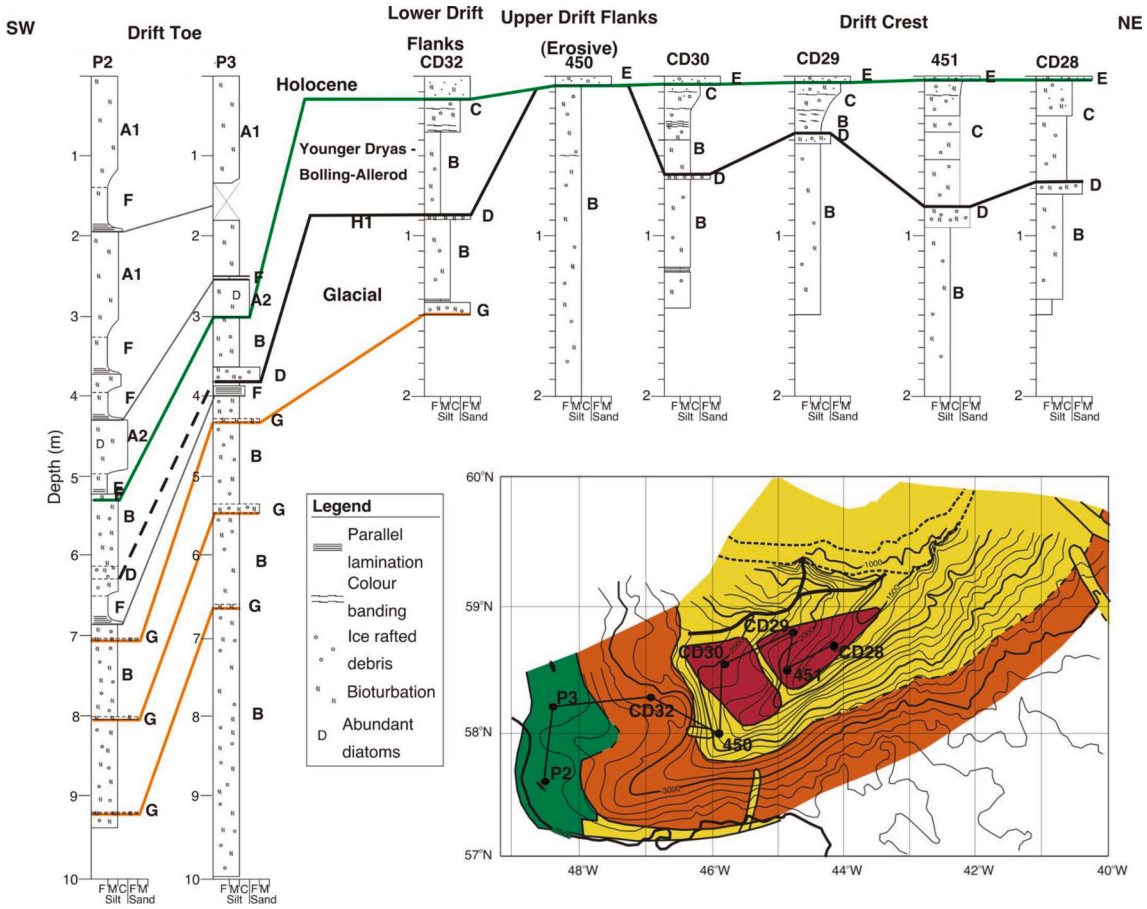

Fig. 11. Graphic sedimentary logs showing the spatial and temporal variations in facies (A1, A2, B to G) of Eirik Drift. Facies codes indicated adjacent to the logs. The inset bathymetric map shows the core locations and the distribution of Holocene sedimentary regimes determined by echocharacter mapping (modified from Hunter et al., 2007a). Yellow - areas of intensive sediment winnowing and erosion; red - areas of moderate sediment winnowing over areas of former contourite deposition; orange - areas of moderate contourite deposition under strong current influence; and green - areas of thick Holocene accumulation. (For interpretation of the references to colour in this figure legend, the reader is referred to the web version of this article.)

proportion of sand (89–90%) and maximum modal grain size (233-234 μm) in two locations; around 2400 m (450) and around 1900 m (451), with a somewhat lower grain size and lower proportion of sand downslope and between these sites (Fig. 14). This spatial variability can be interpreted with reference to the map of depositional regimes. Core 450 lies within the modern high-energy erosional zone associated with the main, moderate-velocity core of the DWBC, while core 451 is significantly shallower, above the present-day DWBC core (Fig. 3). Measured velocities in this crestal area are less than 10 cm/s, lower than those required to erode and transport silt and sand (McCave, 2008). However, we suggest that this spot current measurement does not fully reflect the more typical current regime at this depth, which has been subject to relatively high current activity during the Holocene.

We therefore propose that the shallow crest of the Eirik Drift is subject to significant, short-lived, high-energy events (benthic storms) associated with the EGC. The EGC flows directly across the crest of the drift in this location, including one branch flowing west along the continental slope of Greenland, and a retroflected branch that flows south and then east across Eirik Drift (Holliday et al., 2007). The EGC is associated with significant mesoscale eddy formation further to the north, where the current branches as it exits the Denmark Strait (Håvik et al., 2019). These eddies are associated with significantly higher velocities extending deep into the water column, and are transported hundreds of kilometres southward by the EGC. Such eddies may also form in association with the separation and retroflection of the current above Eirik Drift. Erosion and sediment transport by benthic storms associated with the EGC, rather than the DWBC, may also explain the unusual, N-S trending palaeocurrent measurements at the crest of the drift, with bimodal paleocurrents in 450 perhaps representing the influence of both the EGC and DWBC.

Another, related, mechanism that could explain these elevated velocities at the crest of the drift relate to the East Greenland Spill Jet (EGSJ, Fig. 1). The strength and depth of the EGSJ is directly related to the position of the EGC in relation to the slope, and associated eddies which entrain cold, dense water from the East Greenland Shelf (Pickart et al., 2005; Brearley et al., 2012). Recent observations show that cascading water masses settle at water depths varying between 800 m to >1000 m, and the variability may be significantly higher across longer (Holocene) timescales. These water masses move at significantly higher velocities than the DSOW component of the DWBC, and may episodically erode and transport sediment across the shallower portions of the drift.

Within the deep-water muddy contourite facies, a significant biotic change is observed between sub-facies A2 and A1, suggesting a change in surface oceanographic conditions at this time (~10 ka). A high proportion of large (>100 μm) centric, discoid diatoms (*Thalassiosira* sp.) is present in the early Holocene (sub-facies A2), which are superseded by an assemblage of smaller discoid and spine-shaped forms (*Thalassiothrix longissima* and *Rhizosolenia* sp.) in the later Holocene (sub-facies A1). This later assemblage corresponds to the subarctic assemblage mapped in the area by Andersen et al. (2004). The assemblage in sub-facies A2 correlates approximately in time with an early Holocene (11–9.5 ka) diatom event recorded in the Reykjanes Ridge area (Andersen et al., 2004), which those authors interpret as reflecting exceptionally strong

Table 4
Variation in approximate sedimentation rates for the Holocene, deglacial and glacial sequences across the drift, calculated based on the thickness of the sequences. X = sequence absent. Areas of elevated sedimentation rate are highlighted in grey.

	Approximate sediment rate									
	SW NE									
Core	P2*	P3*	013‡	CD32	011 ‡	450	CD30	CD29	451	CD28
Water Depth (m)	3518	3492	3380	3072	2805	2326	2440	2145	1927	1625
Holocene	32	23	32	1.3	2.3	0.4	0.4	0.25	0.25	0.25
Deglacial	22	20		24		X	18.6	10.6	26.6	21
Glacial			10-15		15	28				

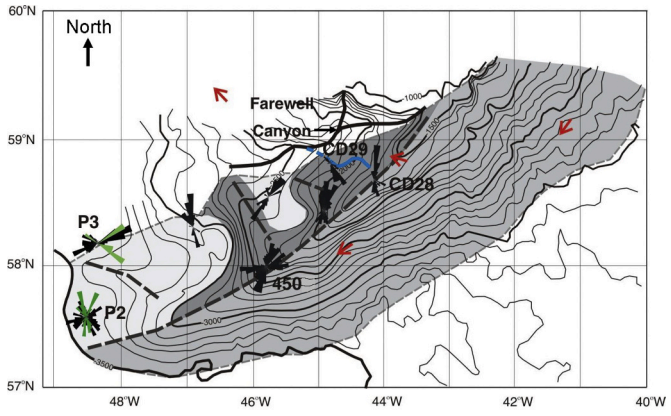

Fig. 12. Rose diagrams indicating the paleocurrent directions at each of the core sites, based on paleomagnetic measurements - i.e. the anisotropy of magnetic susceptibility (AMS) and reorientation of cores using magnetic declination. For cores P2 and P3, the directions shown in green represent samples from turbidites. The red arrows show modern bottom current directions as determined from spot current measurements (Rabinowitz and Eittreim, 1974). The blue line marks the position of a possible tributary channel leading to the Farewell Canyon, as identified in this study. (For interpretation of the references to colour in this figure legend, the reader is referred to the web version of this article.)

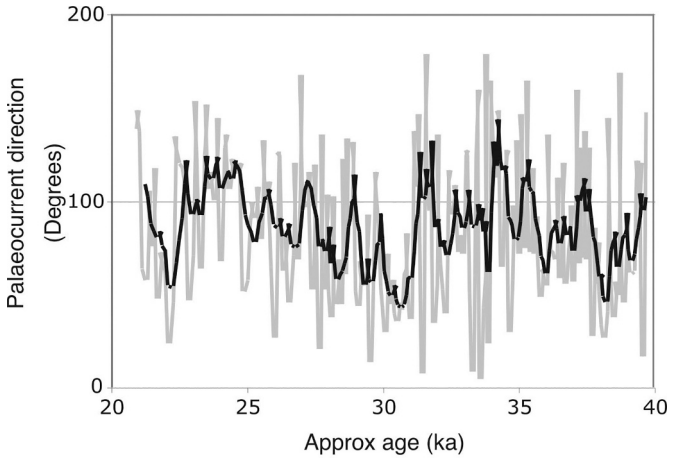

Fig. 13. Downcore variations in paleocurrent direction (y axis) in core 450. The black line represents a 3-point moving average of the data. The age frame (x-axis) is based on radiocarbon dating and correlation of the magnetic susceptibility record with GISP2 oxygen isotope records.

convergence of surface waters in the North West Atlantic related to the presence of the Sub-Arctic Front somewhat further west than its modern position. It is possible that the unusual early Holocene diatom assemblage at the toe of the Eirik Drift, toward centre of Labrador Sea, relates to a stronger influence of arctic surface waters in this area during the Early Holocene.

5.3.2. Deglacial sequence

The deglacial interval shows considerable spatial and temporal variability in facies across the drift (Fig. 15). An increase in the proportion of IRD (>150 μm fraction) occurs with both decreasing water depth and with time. The lower part of this interval, approximately corresponding to the Bolling-Allerod, shows an increasing proportion of IRD to the east, toward the Greenland margin, while the upper part of the deglacial interval, approximately corresponding to the Younger Dryas, is characterised by a high proportion of IRD across the drift. This pattern suggests a supply of IRD from a surface current analogous to the modern EGC during the Bolling-Allerod, with significant ice rafting becoming more widespread into the Younger Dryas.

The evidence for the strength of the bottom currents during this interval is variable. On the upper drift (cores 451 and CD28), a winnowed grain size profile, moderately high modal grain size and moderate to

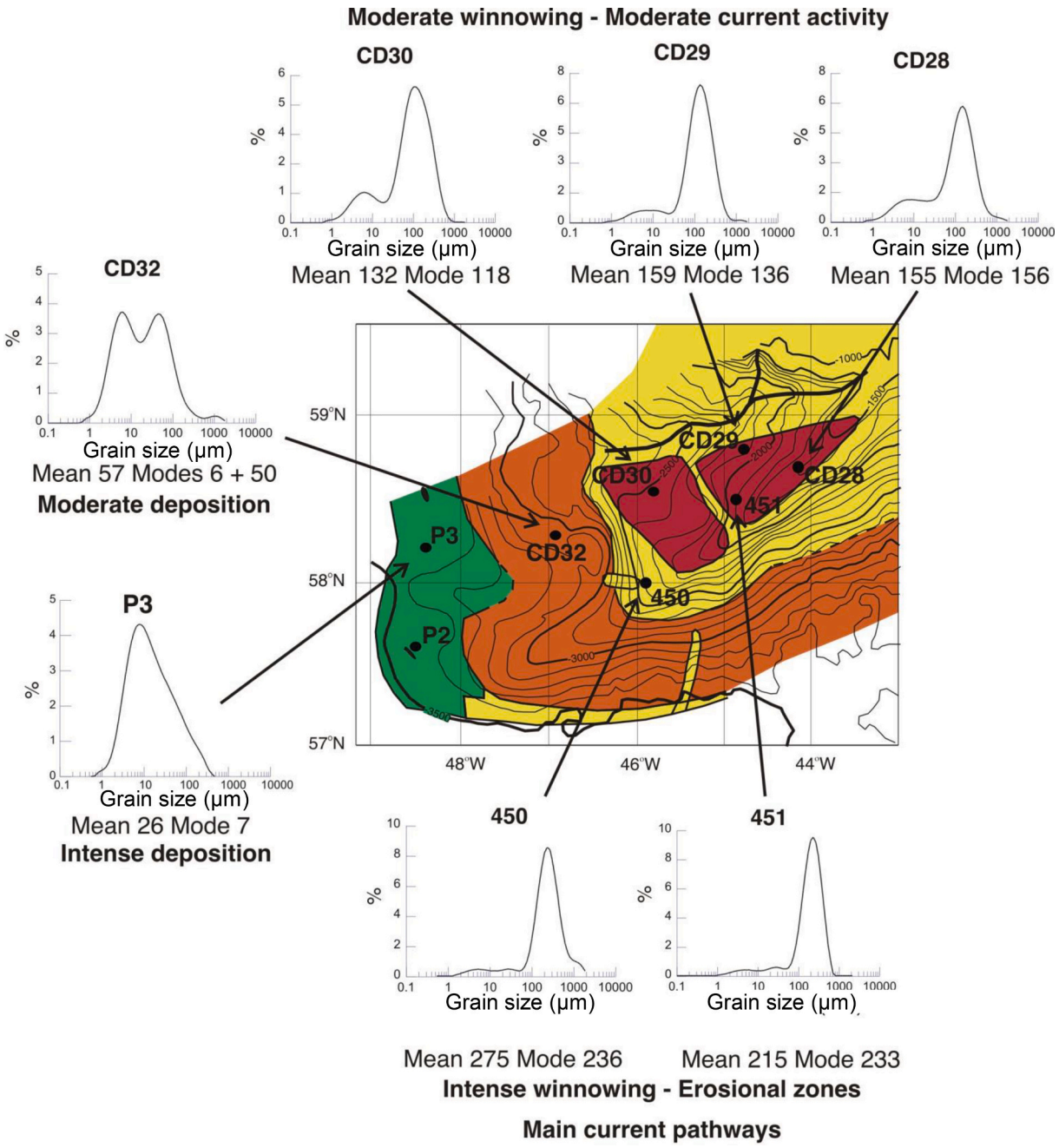

Fig. 14. Spatial and temporal variation in grain size through the Holocene interval, and relationship to the sedimentological zones and current pathways identified from echocharacter mapping (modified from Hunter et al., 2007a). Yellow - areas of intensive sediment winnowing and erosion; red - areas of moderate sediment winnowing over areas of former contourite deposition; orange - areas of moderate contourite deposition under strong current influence; and green - areas of thick Holocene accumulation. (For interpretation of the references to colour in this figure legend, the reader is referred to the web version of this article.)

high P′ suggest significant current activity. A higher proportion of fine material on the drift toe to drift flanks (P2, CD29 to 32) suggests somewhat weaker current activity, although P′ is still moderately high in places. P′ decreases into the Younger Dryas interval in some, but not all cores, although the grain size generally increases due to an increase in the proportion of IRD. These observations suggest that the surface currents were active during this deglacial interval, but that deep thermohaline circulation was inhibited by the influx of fresh water from deglaciation.

Within the Heinrich Event 1 interval (Fig. 16), P` is generally very low (~1.005) across the whole of the drift suggesting little to no current influence on deposition. This interval is therefore interpreted to reflect direct ice-rafted deposition with little to no current influence, consistent with a shutdown in deep circulation (Rahmstorf, 2002; Stanford et al., 2011), and possibly also the surface EGC, at this time.

5.3.3. *Glacial sequence*

Within the late glacial sequence both the mean and modal grain size and P` are generally low, suggesting weak current activity (Fig. 16). However, the modal grain size and P` increase with progressively shallower water depths from the toe to the crest of the drift, suggesting an increase in current strength at shallower depths. The maximum modal grain size and maximum degree of grain alignment occur in core CD28 on the drift crest, where the water depth is around 1600 m. This is consistent with the depth of Glacial North Atlantic Intermediate Water (GNAIW) (Lynch-Stieglitz et al., 2007), and therefore provides further

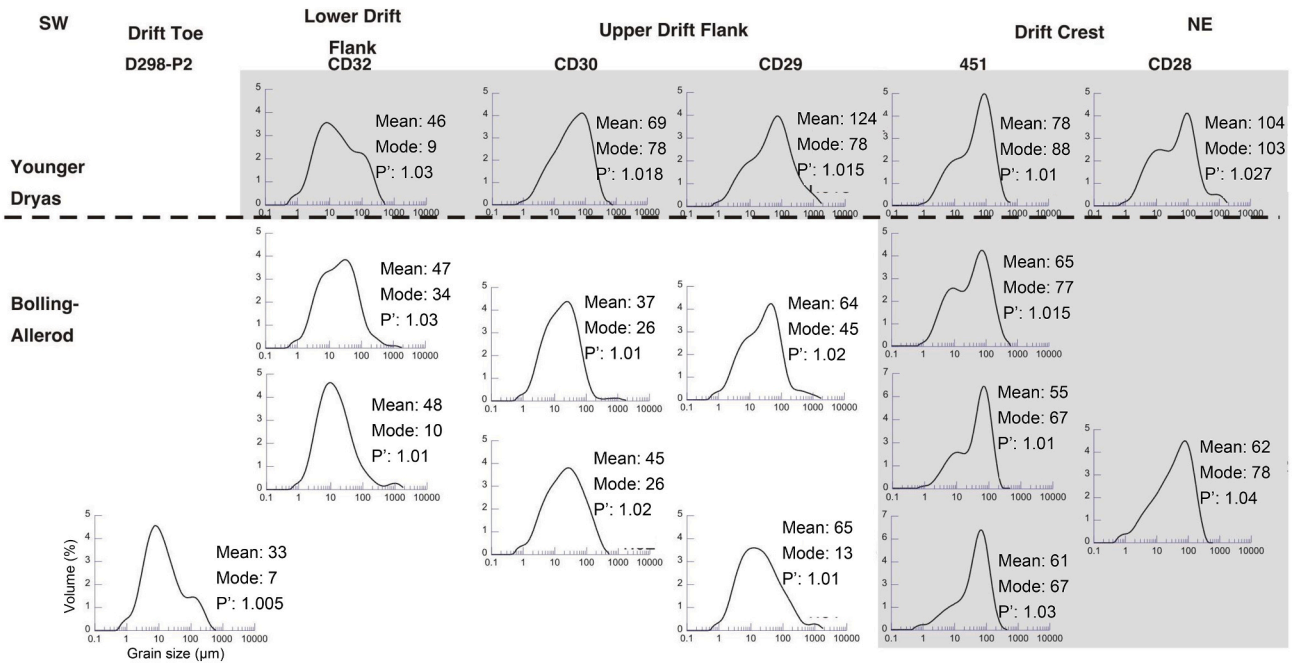

Fig. 15. Spatial and temporal variation in grain size through the deglacial interval. Data shows grain-size distribution, mean, mode and degree of magnetic anisotropy (P′). Grain size distribution plots with a grey background are Facies C sandy muds with abundant IRD, and those with no shading are Facies B sandy muds with scattered IRD.

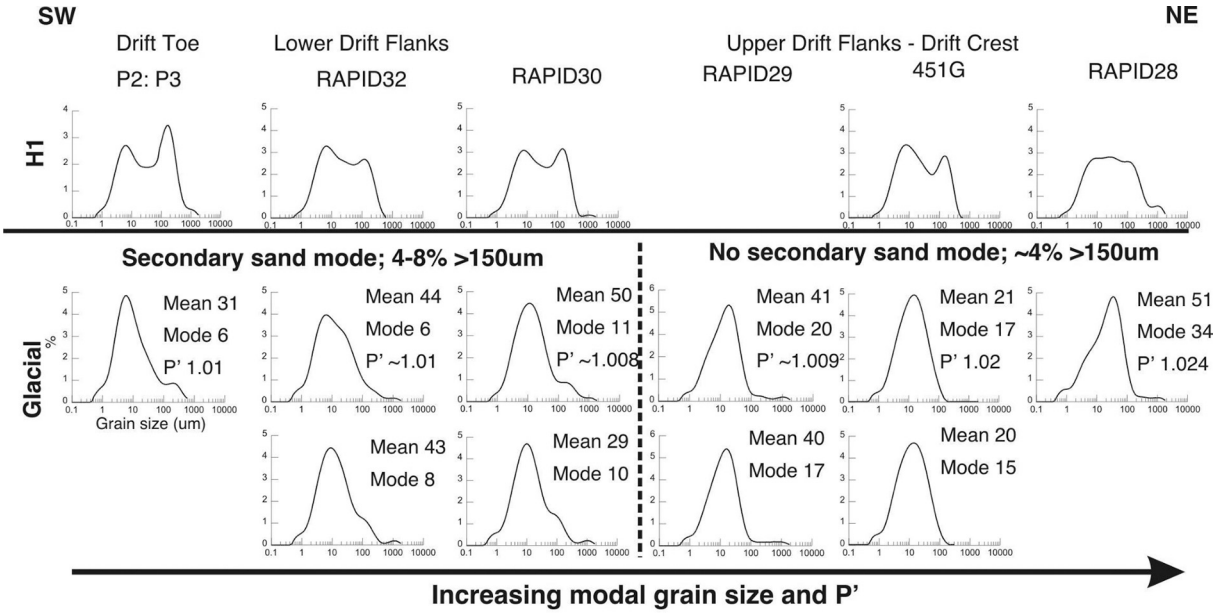

Fig. 16. Spatial and temporal variation in grain size through the late glacial and Heinrich Event 1 intervals. Data shows grain-size distribution, mean, mode and degree of magnetic anisotropy (P′).

support for the hypothesis of a significant, but relatively shallow southward flowing limb of the THC in the North Atlantic during the glacial (Rahmstorf, 2002 and references therein). Alternatively, this may represent sediment transported by benthic storms associated with the EGC, as proposed above. Furthermore, palaeocurrent data from core 450 suggest centennial and millennial scale variability in current strength that may relate to wider palaeoceanographic and palaeoclimatic change during this time.

Further assessment of the degree of bottom current influence across the drift can be made based on the spatial variation in sediment composition and sedimentation rate. Firstly, values of Rb/Sr are lower on the upper drift (0.15–0.3) compared to the drift toe (~0.3–0.4), suggesting a stronger basaltic/MOR influence at shallower levels (Fig. 6). In addition, the sedimentation rate is significantly higher on the upper drift compared to the drift toe (Table 4) and the proportion of IRD is higher in deeper water sites (Fig. 14).

The higher proportion of IRD in deeper water areas (largely below ~2500 m) on the western Eirik Drift could be interpreted as reflecting a higher degree of ice-rafted deposition in this area (and would be consistent with the more continental/cratonic sediment provenance seen in this area). The GLAMAP 2000 reconstruction of sea surface temperature during the last glacial maximum (LGM) shows the whole of

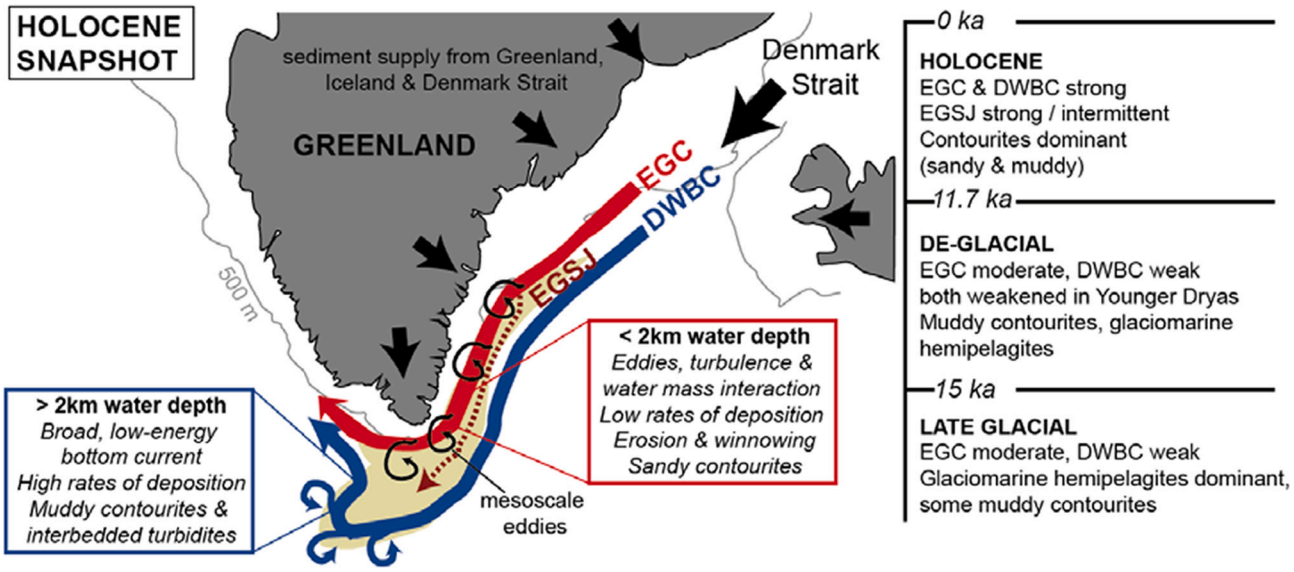

Fig. 17. Summary model for growth and development of the Eirik Drift through Late Glacial, De-glacial and Holocene time intervals. The map shows a snapshot for the present-day with principal currents, current interaction and sediment supply.

the Eirik Drift area to be ice free during the glacial summer, with an assumed cold surface current, analogous to the modern East Greenland Current (EGC), flowing parallel to the Greenland margin (Sarnthein et al., 2003). The modern EGC overlies the upper flanks of the Eirik Drift (largely above depths of around 2500 m), within around 200 km of the Greenland margin (Holliday et al., 2007) and provides a significant source of IRD within this area (Hunter et al., 2007a, 2007b). The higher proportion of IRD in sediments further to the west of this during the glacial interval, largely below 2500 m and more than 200 km from the coast, may suggest this current was displaced further from the coast during this interval. This seems unlikely however, as there is no evidence for a significant width of permanent sea ice around the southern margin of Greenland (i.e. 200 km width) that could have displaced the current (Sarnthein et al., 2003).

A more likely explanation for this compositional variability would be the addition of a source of laterally advected sediment to the upper drift flanks, leading to a relative dilution of the IRD content. This would be consistent both the higher sedimentation rate observed at shallower levels and with the more basaltic Rb/Sr signature at the crest of the drift, assuming that the GNAIW and/or the EGC transported basaltic-derived sediment southward in a similar manner to the modern DSOW and ISOW (Kissel et al., 1999).

5.3.4. Summary model

A summary model for growth and development of the Eirik Drift is shown in Fig. 17. Several different current systems are involved in drift construction, including the Deep Water Boundary Current, East Greenland Current and East Greenland Spill Jet, and their relative strengths have evolved through the Late Glacial, De-glacial and Holocene epochs. Interaction between these different water masses, downward propagating mesoscale eddies and turbulence, lead to high-energy bottom conditions, low-rates of deposition, erosion and winnowing of the sediments, and the deposition of sandy contourites on the eastern flank and crest of the drift. Lower-energy bottom conditions beneath the broad DWBC as it rounds the drift toe lead to high rates of deposition and muddy contourites. Here, they are interbedded with turbidites from South Greenland and debrites from the Canadian margin. The provenance of Eirik Drift contourites includes terrigenous sediment supply from Greenland, Iceland and the Denmark Strait, as well as pelagic biogenic and glaciomarine hemipelagic material.

6. Conclusions

This study shows significant lateral and vertical facies variations within the Eirik Drift, that highlight important changes in the current systems under which the drift formed. Holocene sediments are formed under the influence of both the DWBC and EGC, resulting in a mud-rich toe region with high sediment accumulation rates, and a coarse-grained, winnowed crest and upper flank regions that likely represent benthic storms associated with the EGC, or a fast-flowing episodic core of the EGSJ. Deglacial sediments are mainly mud-rich contourites across the drift, showing that deep thermohaline circulation in the DWBC was inhibited, but that the EGC remained active. During the Heinrich event, even the EGC appears to have reduced in intensity and activity. Glacial sediments show that currents were generally weak, with sedimentation dominated by ice-rafted debris, glaciomarine hemipelagites and muddy contourites, but with greater current influence at shallower depths, consistent with a moderate EGC and weak DWBC. As far as we know, this is the first time that the EGC is inferred to have had a significant role in sedimentation on the Eirik Drift.

Data availability

Grain size, smear slide, geochemical and paleomagnetic data are all recorded in: S. Hunter (2008) *Spatial and temporal variation in contourite sedimentation: link to variations in paleocirculation,* PhD thesis, Southampton University. Core materials are held at the BOSCORF facility, National Oceanography Centre: www.boscorf.org. Shipboard data are documented in cruise reports: Bacon (2006), Kenyon et al. (2004), and McCave (2004) (see reference list).

Declaration of Competing Interest

None.

Acknowledgements

This study was funded as part of the NERC Rapid Climate Change Program under grants NER/T/S/2002/00453 and NER/T/S/2002/00436. The authors wish to thank all those associated with cruises D298, CD159 and TTR-13. The TTR-13 cruise was organised as part of the UNESCO Training Through Research program. The cores used in this

study are stored at BOSCORF at the National Oceanography Centre, Southampton and the authors gratefully acknowledge the use of the BOSCORF facilities. The samples for radiocarbon dating used in this study were analysed at the NERC radiocarbon laboratory in East Kilbride. The authors also wish to thank Dr. Chris Rowan for his assistance in the measurement and interpretation of the palaeomagnetic data. DS and UN thank Heriot-Watt University for general research support. We also thank the reviewers for their attention to detail, which has helped improve the paper considerably.

References

Aksu, A.E., Hillaire-Marcel, C., 1989. Upper Miocene to Holocene oxygen and carbon isotope stratigraphy of sites 646 and 647, Labrador Sea. In: Srivastava, S.P., Arthur, M., Clement, B. (Eds.), Proceedings of the Ocean Drilling Program, Scientific Results. Ocean Drilling Program, College Station, TX, pp. 698–704, 105.

Aksu, A.E., de Vernal, A., Mudie, P.J., 1989. High-resolution foraminfera, palynologic and stable isotopic records of upper Pleistocene sediments from the Labrador Sea: paleoclimatic and paleoceanographic trends. In: Srivastava, S.P., Arthur, M., Clement, B. (Eds.), Proceedings of the Ocean Drilling Program, Scientific Results. Ocean Drilling Program, College Station, TX, pp. 617–652, 105.

Almansi, M., Haine, T.W.N., Gelderloos, R., Pickart, R.S., 2020. Evolution of Denmark strait overflow cyclones and their relationship to overflow surges. Geophys. Res. Lett. 47 (4).

Alvarez, M., Perez, F.F., Bryden, H., Rios, A.F., 2004. Physical and biogeochemical transports in the North Atlantic subpolar gyre. J. Geophys. Res. 109 (C03027).

Andersen, C., Koc, N., Moros, M., 2004. A highly unstable Holocene climate in the subpolar North Atlantic: evidence from diatoms. Quat. Sci. Rev. 23, 2155–2166.

Andrews, J.T., Tedesco, K., 1992. Detrital carbonate-rich sediments, Northwest Labrador Sea: implications for ice-sheet dynamics and iceberg rafting (Heinrich) events in the North Atlantic. Geology 20, 1087–1090.

Andrews, J.T., Smith, L.M., Preston, R., Cooper, T., Jennings, A.E., 1997. Spatial and temporal patterns of iceberg rafting (IRD) along the East Greenland, ca. 68oN, over the last 14 cal. ka. J. Quat. Sci. 12 (1), 1–13.

Arthur, M., Srivastava, S.P., Kaminski, M., Jarrard, R., Osler, J., 1989. Seismic stratigraphy and history of deep circulation and sediment drift development in the Baffin Bay and the Labrador Sea. Proceedings of the Ocean Drilling Program. Sci. Res. [Srivastava, S. P., Arthur, M., Clement, B.et al. College Station, TX, Ocean Drilling Program. 105: 957–988].

Bacon, S., 1997. Circulation and fluxes in the North Atlantic between Greenland and Ireland. J. Phys. Oceanogr. 27 (7), 1420–1435.

Bacon, S., 1998. Decadal variability in the outflow from the Nordic seas to the deep Atlantic Ocean. Nature 394, 871–874.

Bacon, S., 2006. RRS Discovery Cruise 298, 23 Aug - 25 Sep 2005. Cape Farewell and Eirik Ridge (CFER-1). National Oceanography Centre, Southampton, p. 113. Cruise Report No 10.

Bacon, S., Saunders, P.M., 2010. The deep western boundary current at Cape farewell: results from a Moored current meter array. J. Phys. Oceanogr. 40, 815–829.

Ballini, M., Kissel, C., Colin, C., Richter, T., 2006. Deep-water mass source and dynamic associated with rapid climatic variations during the last glacial stage in the North Atlantic: a multiproxy investigation of the detrital fraction of deep-sea sediments. Geochem. Geophys. Geosyst. 7 (2).

Bankole, S., Buckman, J.O., Stow, D.A.V., 2020. Unusual components within a fine-grained contourite deposit: significance for interpretation of provenance and the contourite budget. Minerals 2020 (10), 488.

Bianchi, G.C., McCave, I.N., 1999. Holocene periodicity in North Atlantic climate and deep-ocean flow south of Iceland. Nature 397, 515–517.

Brackenridge, R.E., Stow, D.A.V., Hernández-Molina, F.J., Jones, C., Mena, A., Alejo, I., Ducassou, E., Llave, E., Ercilla, G., Nombela, M.A., Perez-Arlucea, M., Frances, G., 2018. Textural characteristics and facies of sand-rich contourite depositional systems. Sedimentology 65, 2223–2252. https://doi.org/10.1111/sed.12463.

Brearley, J.A., Pickart, R.S., Valdimarsson, H., Jonsson, S., Schmitt, R.W., Haine, T.W., 2012. The East Greenland boundary current system south of Denmark Strait. Deep-Sea Res. I Oceanogr. Res. Pap. 63, 1–19.

Bridge, J.S., Demicco, R.V., 2008. Earth Surface Processes, Landforms and Sediment Deposits. Cambridge University Press, p. 815.

Broecker, W.S., 1991. The great ocean conveyor. Oceanography 4, 79–89.

Chough, S.K., Hesse, R., 1985. Contourites from the Eirik Drift, south of Greenlnd. Sediment. Geol. 41, 185–189.

Compton, R.R., 1962. Manual of Field Geology. John Wiley and Sons, Inc., New York.

Cremer, M., 1989. Texture and microstructure of Neogene-Quaternary sediments, ODP sites 645 and 646, Baffin Bay and Labrador Sea. Proceedings of the Ocean Drilling Program. Sci. Res. Srivastava, S. P., Arthur, M., Clement, B.et al. College Station, TX, Ocean Drilling Program. 105: 7–20.

Croudace, I.W., Rindby, A., Rothwell, R.G., 2006. ITRAX: description and evaluation of a new multi-function X-ray scanner. In: Rothwell, R.G. (Ed.), New Techniques in Sediment Core Analysis, 267. The Geological Society of London. Special Publications, pp. 51–63.

Denk, T., Grímsson, F., Zetter, R., Símonarson, L.A., 2011. The Biogeographic History of the Iceland–North Atlantic Land Bridge Revisited, Late Cenozoic Floras of Iceland. Springer, pp. 647–668.

Dickson, R.R., Brown, J., 1994. The production of North Atlantic deep water: sources, rates and pathways. J. Geophys. Res. 99 (C6), 12,319–12,341.

Fagel, N., Innocent, C., Stevenson, R.K., Hillaire-Marcel, C., 1999. Deep circulation changes in the Labrador Sea since the last Glacial Maximum: new constraints from Sm-Nd data on sediments. Paleoceanography 14 (6), 777–788.

Fagel, N., Innocent, C., Gariepy, C., Hillaire-Marcel, C., 2002. Sources of Labrador Sea sediments since the last glacial maximum inferred from Nd-Pb isotopes. Geochim. Cosmochim. Acta 66 (14), 2569–2581.

Faugères, J.C., Stow, D.A.V., 2008. Contourite drifts: Nature, evolution and controls. In: Rebesco, M., Camerlenghi, A. (Eds.), Contourites, Developments in Sedimentology Series, 60. Elsevier, pp. 259–288.

Faugères, J.C., Stow, D.A.V., Imbert, P., Viana, A., 1999. Seismic features diagnostic of contourite drifts. Mar. Geol. 162, 1–38.

Fichefet, T., Poncin, C., Goosse, H., Huybrechts, P., Janssens, I., Le Treut, H., 2003. Implications of changes in freshwater flux from the Greenland ice sheet for the climate of the 21st century. Geophys. Res. Lett. 30 (17).

Flood, R.D., Kent, D.V., Shor, A.N., Hall, F.R., 1985. The magnetic fabric of surficial deep-sea sediments in the HEBBLE area (Nova Scotian continental rise). Marine Geology 66, 149–167.

Gonthier, E., Faugères, J.C., Stow, D.A.V., 1984. Contourite facies of the Faro Drift. In: Gulf of Cadiz, D.A.V., Stow, D.J.W. (Eds.), Piper Fine-Grained Sediments: deep-water processes and facies Geol. Soc. Lond. Spec. Publ. 15, pp. 275–292.

Hall, I.R., Bianchi, G.C., Evans, J.R., 2004. Centennial to millennial scale Holocene climate-deep water linkage in the North Atlantic. Quat. Sci. Rev. 23, 1529–1536.

Håvik, L., Almansi, M., Våge, K., Haine, T.W., 2019. Atlantic-origin overflow water in the east Greenland current. J. Phys. Oceanogr. 49 (9), 2255–2269.

Hesse, R., Khodabakhsh, S., 1998. Depositional facies of late Pleistocene Heinrich events in the Labrador Sea. Geology 26 (2), 103–106.

Hillaire-Marcel, C., de Vernal, A., Bilodeau, G., Wu, G., 1994. Isotope stratigraphy, sedimentation rates, deep circulation and carbonate events in the Labrador Sea during the last ~200ka. Can. J. Earth Sci. 31, 63–89.

Hinz, K., Schluter, H.-U., Grant, A.C., Srivastava, S.P., Umpleby, D., Woodside, J., 1979. Geophysical transects of the Labrador Sea: labrador to Southwest Greenland. Tectonophysics 59, 151–183.

Hiscott, R.N., Cremer, M., Aksu, A.E., 1989. Evidence from sedimentary structures for processes of sediment transport and deposition during the post-Miocene time at sites 645, 646 and 647, Baffin Bay and the Labrador Sea. In: Srivastava, S.P., Arthur, M., Clement, B., et al. (Eds.), Proceedings of the Ocean Drilling Program 105, Scientific Results, pp. 53–63.

Hohbein, M.W., Sexton, P.F., Cartwright, J.A., 2012. Onset of North Atlantic Deep water production coincident with inception of the Cenozoic global cooling trend. Geology 40, 255–258.

Holliday, N.P., Meyer, A., Bacon, S., Alderson, S.G., de Cuevas, B., 2007. Retroflection of part of the East Greenland current at Cape Farewell. Geophys. Res. Lett. 34 (L07609) https://doi.org/10.1029/2006GL029085.

Holliday, N.P., Bacon, S., Allen, J., McDonagh, E.L., 2009. Circulation and transport in the Western Boundary Currents at Cape Farewell, Greenland. J. Phys. Oceanogr. 39, 1854–1870.

Hunter, S.E., Wilkinson, D., Rohling, E.J., McCave, I.N., Louarn, E., Stow, D.A.V., 2007a. Hydrography and sedimentation on the Eirik Drift, southern Greenland margin. Deep-Sea Res. 54, 2036–2066.

Hunter, S.E., Wilkinson, D., Stow, D.A.V., Bacon, S., Rohling, E.J., Stanford, J., Kenyon, N.H., Akhmetzhanov, A., 2007b. The Eirik Drift: A longterm barometer of North Atlantic Deep Water flux south of Cape Farewell, Greenland. In: Viana, A., Rebesco, M. (Eds.), Economic and Paleoceanographic Significance of Contourite Deposits, 276. Geological Society, Special Publication, London, pp. 245–264.

Innocent, C., Fagel, N., Stevenson, R.K., Hillaire-Marcel, C., 1997. Sm-Nd signature of the modern and late Quaternary sediments from the Northwest North Atlantic: implications for deep current changes since the last Glacial Maximum. Earth Planet. Sci. Lett. 146, 607–625.

Jakobsson, M., Backman, J., Rudels, B., Nycander, J., Frank, M., Mayer, L., Jokat, W., Sangiorgi, F., O'Regan, M., Brinkhuis, H., King, J., Moran, K., 2007. The early Miocene onset of a ventilated circulation regime in the Arctic Ocean. Nature 447, 986–990.

Johnson, L.G., Schneider, E.D., 1969. Depositional ridges in the North Atlantic. Earth Planet. Sci. Lett. 6 (6), 416–422.

Joseph, L.H., Rea, D.K., van der Pluijm, B.A., 1998. Use of grain size and magnetic fabric analyses to distinguish among depositional environments. Paleoceanography 13 (5), 491–501.

Joseph, L.H., Rea, D.K., van der Pluijm, B.A., Gleason, J.D., 2002. Antarctic environmental variability since the late Miocene: ODP Site 745, the East Kerguelen sediment drift. Earth Planet. Sci. Lett. 201 (1), 127–142.

Kaminski, M.A., Gradstein, F.M., Scott, D.B., MacKinnon, K.D., 1989. Neogene benthic foraminifera biostratigraphy and deep-water history of sites 645, 646 and 647, Baffin Bay and Labrador Sea. Proceed. Ocean Drill. Prog. Scientific Res. [Srivastava, S. P., Arthur, M., Clement, B.et al. College Station, TX, Ocean Drilling Program. 105: 731–756].

Kenyon, N.H., Ivanov, M.K., Akhmetzhanov, A., Kozlova, E.V., Mazzini, A., 2004. Interdisciplinary Studies of North Atlantic and Labrador Sea Margin Architecture and Sedimentary Processes. Preliminary Results of Investigations During the TTR-13 Cruise of RV Professor Logachev, 2003, 68. Intergovernmental Oceanographic Commission Technical Series, UNESCO.

Kissel, C., Laj, C., Labeyrie, L., Dokken, T., Voelker, A., Blamart, D., 1999. Rapid climatic variations during marine isotope stage 3: magnetic analysis of sediments form Nordic Seas and North Atlantic. Earth Planet. Sci. Lett. 171, 489–502.

Knutz, P.C., 2008. Paleoceanographic significance of contourite drifts. In: Rebesco, M., Camerlenghi, A. (Eds.), Contouritese, Developments in Sedimentology Series, 60. Elsevier, pp. 5011–5535.
Lackschewitz, K.S., Wallrabe-Adams, H.J., Garbe-Schönberg, D., 1994. Geochemistry of surface sediments from the mid-oceanic Kolbeinsey Ridge, north of Iceland. Mar. Geol. 121 (1–2), 105–119.
Lauderdale, J.M., Bacon, S., Naveira Garabato, A.C., Holliday, N.P., 2008. Intensified turbulent mixing in the boundary current system of southern Greenland. Geophys. Res. Lett. 35, L04611.
Lenaerts, J.T., Le Bars, D., Van Kampenhout, L., Vizcaino, M., Enderlin, E.M., Van Den Broeke, M.R., 2015. Representing Greenland ice sheet freshwater fluxes in climate models. Geophys. Res. Lett. 42 (15), 6373–6381.
Linthout, K., Troelstra, S.R., Kuijpers, A., 2000. Provenance of coarse ice-rafted detritus near the SE Greenland margin. Neth. J. Geosci. 79 (1), 109–121.
Lynch-Stieglitz, J., Adkins, J.F., Curry, W.B., Dokken, T., Hall, I.R., Herguera, J.C., Hirschi, J.J.-M., Ivanova, E.V., Kissel, C., Marchal, O., Marchitto, T.M., McCave, I.N., McManus, J., Mulitza, S., Ninnemann, U., Peeters, F., Yu, E.-F., Zahn, R., 2007. Atlantic meridional overturning circulation during the last Glacial Maximum. Science 316, 66–69.
McCartney, M., 1992. Recirculating components of the deep boundary current of the northern North Atlantic. Prog. Oceanogr. 29, 283–382.
McCave, I.N., 2004. R.R.S. Charles Darwin Cruise 159 1st - 30th July 2004, Fairlie. Scotland to St John's, Newfoundland.
McCave, I.N., 2008. Size Sorting During Transport and Deposition of Fine Sediments. In: Rebesco, M., Camerlenghi, A. (Eds.), Developments in Sedimentology. Elsevier, Contourites, pp. 121–142.
McCave, I.N., Tucholke, B.E., 1986. Deep current-controlled sedimentation in the western North Atlantic. In: Vogt, P.R., Tucholke, B.E. Boulder (Eds.), The Geology of North America, Vol. M. Co, Geological Society of America, Western Atlantic Region, pp. 451–468.
McCave, I.N., Hall, I.R., Bianchi, G.G., 2006. Laser vs. settling velocity differences in silt grain size measurements: estimation of palaeocurrent vigour. Sedimentology 53, 919–928.
Müller-Michaelis, A., Uenzelmann-Neben, G., 2014. Development of the Western Boundary Undercurrent at Eirik Drift related to changing climate since the early Miocene. Deep-Sea Res. I Oceanogr. Res. Pap. 93, 21–34.
Müller-Michaelis, A., Uenzelmann-Neben, G., Stein, R., 2013. A revised early Miocene age for the instigation of the Eirik Drift, offshore southern Greenland: evidence from high-resolution seismic reflection data. Mar. Geol. 340 https://doi.org/10.1016/j.margeo.2013.04.012.
Myhre, A., Thiede, J., Firth, J., 1995a. North Atlantic-Arctic Gateways. Proceedings Ocean Drilling Program Initial Reports.
Myhre, A., Thiede, J., Firth, J., Ahagon, N., Black, K., Bloemendal, J., Brass, G., Bristow, J., Chow, N., Cremer, M., 1995b. Site 909, Proceedings of the Ocean Drilling Program. Initial reports. Ocean Drill. Prog. 159–220.
Nicholson, U., Stow, D.A.V., 2019. Erosion and deposition beneath the Subantarctic Front since the early Oligocene. Nat. Sci. Rep. 9, 1–9.
Nicholson, U., Libby, S., Tappin, D.R., McCarthy, D., 2020. The Subantarctic Front as a sedimentary conveyor belt for tsunamigenic submarine landslides. Mar. Geol. 424, 106161.
Nishida, N., Itaki, T., Amano, A., Katayama, H., Sato, T., Stow, D.A.V., Nicholson, U., 2021. The Ryuku Contourite Sand Sheet: Contourite formation beneath the Kuroshio current, North-Western Pacific Ocean. Mar. Geol. (in press).
Pickart, R.S., Moore, G.W.K., Torres, D.J., Fratantoni, P.S., Goldsmith, R.A., Yang, J., 2005. Upwelling on the continental slope of the Alaskan Beaufort Sea: storms, ice, and oceanographic response. J. Geophys. Res. Oceans 114 (C1).
Poore, H., Samworth, R., White, N., Jones, S., McCave, I., 2006. Neogene overflow of Northern Component Water at the Greenland- Scotland Ridge. Geochem. Geophys. Geosyst. 7.
Rabinowitz, P.D., Eittreim, S.L., 1974. Bottom current measurement in the Labrador Sea. J. Geophys. Res. 79 (27), 4085–4090.
Rahmstorf, S., 2002. Ocean circulation and climate during the past 120,000 years. Nature 419, 207–214.
Rahmstorf, S., 2006. Thermohaline ocean circulation. In: Elias, S.A. (Ed.), Encyclopedia of Quaternary Sciences. Elsevier, Amsterdam.
Ramsay, A.T., Smart, C.W., Zachos, J.C., 1998. A model of early to middle Miocene deep ocean circulation for the Atlantic and Indian Oceans. Geol. Soc. Lond., Spec. Publ. 131, 55–70.
Rees, A.I., 1965. The use of anisotropy of magnetic susceptibility in the estimation of sediment fabric. Sedimentology 4, 257–271.
Sarnthein, M., Pflaumann, U., Weinelt, M., 2003. Past extent of sea ice in the northern North Atlantic inferred from foraminiferal paleotemperature estimates. Paleoceanography 18 (2), 1047. https://doi.org/10.1029/2002PA00071.
Schlitzer, R., 2020. Ocean data view. ODV 5 (2), 1. http://odv.awi.de.
Srivastava, S.P., Arthur, M., Clement, B., 1989a. Proceeding of the Ocean Drilling Program, Scientific Results, vol. 105. Ocean Drilling Program, College Station, TX.
Srivastava, S.P., Louden, K.E., Chough, S.K., Mosher, D., Loncarevic, B.D., Mudie, P.J., de Vernal, A., MacLean, B., 1989b. Results of detailed geological and geophysical measurement at ODP Sites 645 in Baffin Bay and 646 and 647 in the Labrador Sea. Proceed. Ocean Drill. Prog. Scientific Results [Srivastava, S. P., Arthur, M., Clement, B. et al. College Station, TX, Ocean Drilling Program. 105: 891–919].
Stanford, J., Rohling, E.J., Hunter, S.E., Roberts, A.P., Rasmussen, S.O., Bard, E., McManus, J., Fairbanks, R.G., 2006. Timing of meltwater pulse 1a and climate responses to meltwater injections. Paleoceanography 21 (4), PA4103.
Stanford, J.D., Hemingway, R., Rohling, E.J., Challenor, P.G., Medina-Elizalde, M., Lester, A.J., 2011. Sea-level probabilities for the last deglaciation: a statistical analysis of far-field records. Glob. Planet. Chang. 79, 193–203.
Stoner, J.S., Channell, J.E.T., Hillaire-Marcel, C., 1995. Magnetic properties of deep-sea sediments off Southwest Greenland: evidence for major differences between the last two deglaciations. Geology 23 (3), 241–244.
Stoner, J.S., Channell, J.E.T., Hillaire-Marcel, C., 1996. The magnetic signature of rapidly deposited detrital layers from the deep Labrador Sea: relationship to North Atlantic Heinrich layers. Paleoceanography 11 (3), 309–325.
Stow, D.A.V., Faugères, J.C., 2008. Contourite facies and development of the facies model. In: Rebesco, M., Camerlenghi, A. (Eds.), Contourites, Developments in Sedimentology Series, 60. Elsevier, pp. 223–256.
Stow, D.A.V., Hernandez-Molina, F.J., Llave, E., Bruno, M., García, V., del Rio, Díaz, Somoza, L., Brackenridge, R.E., 2013. The Cadiz Contourite Channel: sandy contourites, bedforms and dynamic current interaction. Marine Geol. 343, 99–114.
Stow, D.A.V., Piper, D.J.W., 1984. Deep-water fine-grained sediments: facies models. In: Stow, D.A.V., Piper, D.J.W. (Eds.), Fine-Grained Sediments: Deep-Water Processes and Facies, 15. Geol. Soc. Lond. Spec. Publ., pp. 611–646
Stow, D.A.V., Smillie, Z., 2020. Distinguishing between deepwater sediment facies: turbidites, contourites and hemipelagites. Geosciences 10 (2), 68.
Stow, D.A.V., Pudsey, C.J., Howe, J.A., Faugeres, J.C., Viana, A., 2002. Bottom currents and contourites: state-of-the-art. In: Stow, D.A.V., et al. (Eds.), Atlas of Deep-water Contourite Systems: Modern Drifts and Ancient Series, Seismic and Sedimentary Characteristics, 22. Geol. Soc. London. Memoir, pp. 7–20.
Stow, D.A.V., Hunter, S., Wilkinson, D., Hernández-Molina, F.J., 2008. The nature of contourite deposition. In: Rebesco, M., Camerlenghi, A. (Eds.), Contourites, Developments in Sedimentology Series, 60. Elsevier, pp. 143–157.
Straume, E.O., Gaina, C., Medvedev, S., Nisancioglu, K.H., 2020. Global Cenozoic Paleobathymetry with a focus on the Northern Hemisphere Oceanic Gateways. Gondwana Res. https://doi.org/10.1016/j.gr.2020.05.011.
Thiede, J., Eldholm, O., 1983. Speculations about the Paleodepth of the Greenland-Scotland Ridge during late Mesozoic and Cenozoic Times. In: Bott, M.H.P., Saxov, S., Talwani, M., Thiede, J. (Eds.), Structure and Development of the Greenland-Scotland Ridge: New Methods and Concepts. Springer US, Boston, MA, pp. 445–456.
Wold, C.N., 1994. Cenozoic sediment accumulation on drifts in the northern North Atlantic. Paleoceanography 9, 1–6.
Wunsch, C., 2002. What is the Thermohaline Circulation? Science 298, 1179–1180.